Chapter 3

Beam Model

"I wish you love and happiness --
I guess I wish you all the best
I wish you don't do like I do and ever --
fall in love with someone like you"
John Prine

3.1 Introduction

In this chapter, equations of motion are developed to describe the response of the simply supported beam treated with WRC(s). Various acoustic responses are obtained to analyze the noise control mechanisms of the passive cell device. The numerical model is used to analyze the mechanical and acoustic effects produced by the weak radiating cells. Fundamental interaction effects such as mass loading, damping, and modal coupling are considered. The acoustic responses include source strength, sound power, and radiation efficiency. To alleviate the drawback of noise produced by the WRC at resonance, several methods to improve the performance of the WRC's at resonance are discussed. Lastly, a wavenumber transform of the cells' responses provides additional insight into the system. Numerical results from this model are used to interpret the noise reduction performance of the WRCs.

3.2 Simply Supported Beam Model

Figure (3.1a) illustrates a beam with three WRCs implemented. The model of the system is shown in Figure (3.1b). The beam's properties are defined by the mass per unit length m_b, the bending stiffness EI, the length L_{bx}, and the width L_{by}. The response of the beam is defined by the continuous function $\tilde{w}(x,t)$. The cells are modeled by assuming the cell's frame to be rigid and the center plate and shim approximated by a single rigid plate with two degree-of-freedoms (dofs), i.e., a translation $y(t)$ and a rotation $\theta(t)$. The cell's frame and the inner plate define the two radiating surfaces S_1 and S_2, respectively. The inner plate, referred to as the cell's plate, has length b, width d, and thickness e. Since the cell's frame is considered rigid, the normal motion of the outer surface S_1 is assumed to have the same response as the beam's response, $\tilde{w}(x,t)$. The effect of the shim and cavity are modeled as two linear springs, one axial, k, and the other torsional, k_t. These springs connect to the rigid element center point and to the beam at the same axial coordinate x. The axial spring constrains the vertical motion $y(t)$ while the torsional spring constrains the rotation $\theta(t)$ of the cell's plate, respectively. Note that the compressibility of the fluid in the cavity only contributes to the axial spring value since the rotation of the cell's plate does not lead to a change in the cavity volume. It is important to note that all the cells have the same dimension, but may have different properties, i.e. natural frequency or damping. Recent experimental work has indicated that the effect of the cell's frame on the based structure is mainly of mass loading, hence no significant increase of the structural stiffness [27]. Thus, the mass of the cell's frame, m_c, is treated as an additional uniformly distributed mass added to the beam. Thus, the total mass per unit length of the beam with the cells is $\tilde{m}_b = m_b + m_c$ while the bending stiffness is not affected.

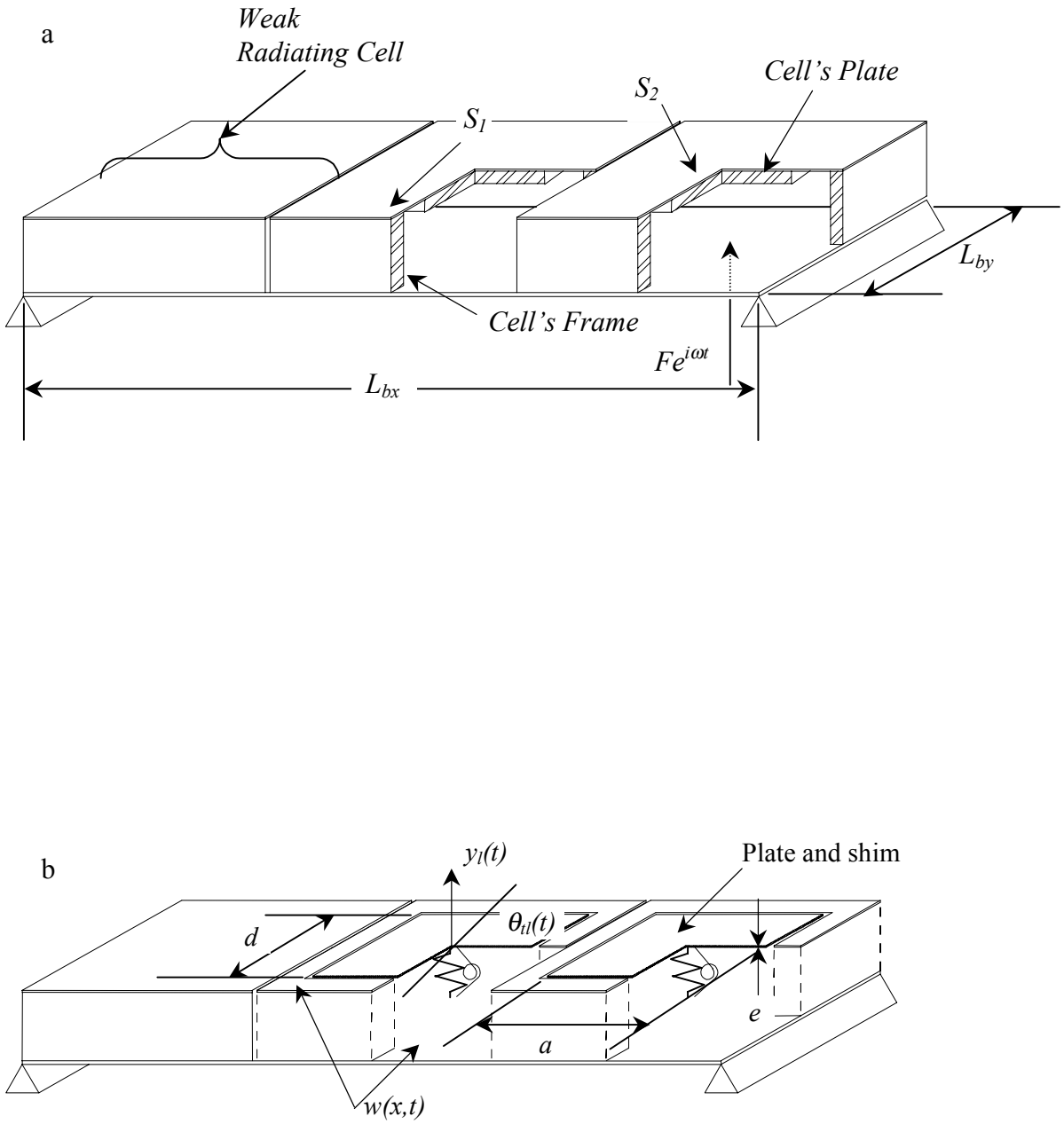

Figure 3.1: (a) Simply supported beam with 3 WRCs and (b) simplified model.

3.3 Equations of Motion

To predict the acoustic performance of the beam-WRCs system, the response of the structure is required. To this end, the response of the continuous beam is expanded in terms of the mode of the uniform simply supported beam with mass per unit length $\widetilde{m}_b$ and bending stiffness *EI*. That is,

$$\widetilde{w}(x,t)=\sum_{n=1}^{N}\widetilde{\Phi}_n(x)\widetilde{q}_n(t) \tag{3.1}$$

where $\widetilde{q}_n(t)$ is the n^{th} modal displacement amplitude at time *t* including the effect of the WRCs, *N* is the number of modes included in the expansion, and $\widetilde{\Phi}_n(x)$ is the n^{th} mass normalized mode shape of a simply supported beam givens as [31]

$$\widetilde{\Phi}_n(x)=\sqrt{\frac{2}{\widetilde{m}_b L_x}}\,sin\left(\frac{n\pi x}{L_x}\right). \tag{3.2}$$

The modes of the beam satisfy the orthogonality conditions

$$\int_o^{L_{bx}}\widetilde{m}_b\widetilde{\Phi}_n(x)\widetilde{\Phi}_s(x)dx=\delta_{ns} \qquad \int_o^{L_{bx}}EI\frac{d^2\widetilde{\Phi}_n(x)}{dx^2}\frac{d^2\widetilde{\Phi}_s(x)}{dx^2}dx=\widetilde{\omega}_n^2\delta_{ns} \tag{3.3a,b}$$

where δ_{ij} is the Dirac delta function; $\widetilde{\omega}_n$ is the n^{th} natural frequency of the beam with mass distribution $\widetilde{m}_b$ and bending stiffness *EI*. That is [31]

$$\widetilde{\omega}_n=\left(\frac{n\pi}{L_{bx}}\right)^2\sqrt{\frac{EI}{\widetilde{m}_b}}. \tag{3.4}$$

Once again, it is important to remark that the beam response $\widetilde{w}(x,t)$ in Eq (3.1) also defines the motion of the surface S_1 of the cells.

The response of the l^{th} cell plate surface S_2 is given in terms of the translation and rotational WRC's dofs,

$$w_l(x,t) = y_l(t) + \theta_l(t)(x - x_l) \quad -a/2 + x_l \le x \le a/2 + x_l \qquad l = 1,..., N_c \tag{3.5}$$

where x_l is the center point location of the l^{th} cell's plate on the beam; *a/2* equals half the length of the WRC's inner plate; and N_c is the number of cells mounted on the structure.

The equations of motion for both beam and plate-WRC systems are determined using Lagrange's formulation

$$\frac{d}{dt}\left(\frac{\partial T}{\partial \dot{u}_i}\right) - \frac{\partial T}{\partial u_i} + \frac{\partial U}{\partial u_i} = F_i \qquad i = 1,2,..., N + 2N_c \tag{3.6}$$

where T and U represent kinetic and potential energies, respectively; u_i is the generalized coordinates and; $\dot{u}_i$ is the generalized velocity. The right side, F_i, is related to all non-conservative forces corresponding to u_i [32]. For the $N + 2N_c$ degree of freedoms system here, the generalized coordinates u_i are

$$u_i(t) = \begin{cases} \tilde{q}_n(t) & n = 1,..., N \\ y_l(t) & l = 1,..., N_c \\ \theta_l(t) & l = 1,..., N_c \end{cases}. \tag{3.7}$$

To derive the equations of motion in terms of $\tilde{q}_n(t)$, $y_l(t)$, and, $\theta_l(t)$, the kinetic energy T, potential energy U, and external work by the non-potential forces F_i are computed and replaced into Eq (3.7).

The kinetic energy T is given as

$$T = \frac{1}{2}\int_0^{L_{bx}} \tilde{m}_b \left(\frac{\partial \tilde{w}}{\partial t}(x,t)\right)^2 dx + \sum_l^{N_c}\left\{\frac{1}{2}M_l\left(\frac{dy_c(t)}{dt}\right)^2 + \frac{1}{2}J_l\left(\frac{d\theta_l(t)}{dt}\right)^2\right\} \tag{3.8}$$

where M_l and J_l are the mass and rotational mass moment of inertia of the l^{th} cell's plate, respectively. The rotational mass moment of inertia is

$$J_l = \frac{M_l}{12}\left(a^2 + e^2\right). \tag{3.9}$$

The potential energy U consists in the form of strain energy from elastic deformation of the beam and cells' springs, which is given as

$$U = \frac{1}{2}\int_0^{L_{bx}} EI\left(\frac{\partial^2 \tilde{w}(x,t)}{\partial x^2}\right)^2 dx + \sum_l^{N_c}\left\{\frac{1}{2}k_l\left[y_l(t) - \tilde{w}(x_l,t)\right]^2 + \frac{1}{2}k_{tl}\left[\theta_l(t) - \frac{d\tilde{w}(x_l,t)}{dx}\right]^2\right\} \tag{3.10}$$

where k_l and k_{tl} are linear and torsional spring stiffness of the l^{th} cell, respectively. Replacing the modal expansion from Eq (3.1) into Eqs (3.8) and (3.10) and using the orthogonality properties of the modes Eqs (3.3a,b) gives

$$T = \frac{1}{2}\sum_{n=1}^{N}\left(\frac{d\tilde{q}_n(t)}{dt}\right)^2 + \sum_l^{N_c}\left\{\frac{1}{2}M_l\left(\frac{dy_l(t)}{dt}\right)^2 + \frac{1}{2}J_l\left(\frac{d\theta_l(t)}{dt}\right)^2\right\} \tag{3.11}$$

and

$$U = \frac{1}{2}\sum_{n=1}^{N}\tilde{\omega}_n^2\tilde{q}_n^2(t) + \sum_l^{N_c}\left\{\frac{1}{2}k_l\left[y_l(t) - \sum_{n=1}^{N}\tilde{\Phi}_n(x_l)\tilde{q}_n\right]^2 + \frac{1}{2}k_{tl}\left[\theta_l(t) - \sum_{n=1}^{N}\frac{d\tilde{\Phi}_n(x_l)}{dx}\tilde{q}_n\right]^2\right\}. \tag{3.12}$$

The generalized force, F_i, for a beam under transverse bending [31] is

$$F_i = \int_0^{L_{bx}} f(x,t)\tilde{\Phi}_n(x)dx \tag{3.13}$$

where $f(x,t)$ is the external forcing function. Here the forcing function acting on the beam is a harmonic point force applied at $x = x_f$. That is

$$f(x,t) = Fe^{i\omega t}\delta\left(x_f - x\right), \tag{3.14}$$

such that after integration of Eq (3.13) gives

$$F_i = F\tilde{\Phi}_n(x_f)e^{i\omega t}. \tag{3.15}$$

Substituting the kinetic, potential, and generalized force equations into the Lagrange's equation leads to

$$\begin{aligned}\frac{d^2\tilde{q}_n(t)}{dt^2} + \tilde{\omega}_n^2\tilde{q}_n(t) - \sum_{l}^{N_c}\left\{k_l\tilde{\Phi}_n(x_l)\left[y_l(t) - \sum_{n=1}^{N}\tilde{\Phi}_n(x_l)\tilde{q}_n(t)\right] + \right. \\ \left. k_{tl}\frac{d\tilde{\Phi}_n(x_l)}{dx}\left[\theta_l(t) - \sum_{n=1}^{N}\frac{d\tilde{\Phi}_n(x_l)}{dx}\tilde{q}_n(t)\right]\right\} = F\tilde{\Phi}_n(x_f)e^{i\omega t}\end{aligned}, \tag{3.16}$$

$$M_l\frac{d^2y_l(t)}{dt^2} + k_l\left[y_l(t) - \sum_{n=1}^{N}\tilde{\Phi}_n(x_l)\tilde{q}_n(t)\right] = 0, \text{ and} \tag{3.17}$$

$$J_l\frac{d^2\theta_l(t)}{dt^2} + k_{tl}\left[\theta_l(t) - \sum_{n=1}^{N}\frac{d\tilde{\Phi}_n}{dx}(x_l)\tilde{q}_n(t)\right] = 0. \tag{3.18}$$

The harmonic steady-state solutions to the equations of motion are $q_n(t) = Q_n e^{i\omega t}$, $y_l(t) = Y_l e^{i\omega t}$, and $\theta_l(t) = \Theta_l e^{i\omega t}$. Thus, the response of the system is obtained from the solution of the linear system of equations

$$[\hat{M}]\{\ddot{u}_i\} + [\hat{K}]\{u_i\} = \{\hat{F}_i\} \tag{3.19}$$

where the mass matrix is

$$\left[\hat{M}\right]=\left[\begin{array}{ccc:ccc:ccc} 1 & 0 & & & & & & & 0 \\ 0 & \ddots & & & & & & & \\ & & 1 & & & & & & \\ \hdashline & & & M_1 & & & & & \\ & & & & \ddots & & & & \\ & & & & & M_{N_c} & & & \\ \hdashline & & & & & & J_1 & \ddots & \vdots \\ & & & & & & \ddots & \ddots & 0 \\ 0 & & & & & & \cdots & 0 & J_{N_c} \end{array}\right]; \tag{3.19a}$$

the stiffness matrix is

$$\left[\hat{K}\right]=\left[\begin{array}{ccc:ccc:ccc} \tilde{\omega}_1^2+K_{11} & \cdots & K_{1N} & -k_1\tilde{\Phi}_1(x_1) & \cdots & -k_{N_c}\tilde{\Phi}_1(x_{N_c}) & -k_{t1}\dfrac{\tilde{\Phi}_1(x_1)}{dx} & \cdots & -k_{N_c}\dfrac{\tilde{\Phi}_1(x_{N_c})}{dx} \\ \vdots & \ddots & & \vdots & \ddots & \vdots & \vdots & \ddots & \vdots \\ K_{N1} & & \tilde{\omega}_N^2+K_{NN} & -k_1\tilde{\Phi}_N(x_1) & \cdots & -k_{N_c}\tilde{\Phi}_N(x_{N_c}) & -k_{t1}\dfrac{\tilde{\Phi}_N(x_1)}{dx} & \cdots & -k_{t N_c}\dfrac{\tilde{\Phi}_N(x_{N_c})}{dx} \\ \hdashline -k_1\tilde{\Phi}_1(x_1) & \cdots & -k_1\tilde{\Phi}_N(x_1) & k_1 & & 0 & & & \\ \vdots & \ddots & \vdots & & \ddots & & & 0 & \\ -k_{N_c}\tilde{\Phi}_1(x_{N_c}) & \cdots & -k_{N_c}\tilde{\Phi}_N(x_{N_c}) & 0 & & k_{N_c} & & & \\ \hdashline -k_{t1}\dfrac{\tilde{\Phi}_1(x_1)}{dx} & \cdots & -k_{t1}\dfrac{\tilde{\Phi}_N(x_1)}{dx} & & & & k_{t1} & & 0 \\ \vdots & \ddots & \vdots & & 0 & & & \ddots & \\ -k_{t N_c}\dfrac{\tilde{\Phi}_1(x_{N_c})}{dx} & \cdots & -k_{t N_c}\dfrac{\tilde{\Phi}_N(x_{N_c})}{dx} & & & & 0 & & K_{t N_c} \end{array}\right] \tag{3.19b}$$

where

$$K_{sr}=\sum_{l=1}^{N_c}\left\{k_l\tilde{\Phi}_s(x_l)\tilde{\Phi}_r(x_l)+k_{tl}\frac{d\tilde{\Phi}_s(x_l)}{dx}\frac{d\tilde{\Phi}_r(x_l)}{dx}\right\} \qquad s,r=1,...,N\,, \tag{3.19b$_1$}$$

and the external force vector is

$$\left\{\hat{F}_i\right\}=\left[F\tilde{\Phi}_1(x_f) \quad \cdots \quad F\tilde{\Phi}_N(x_f) \;\vdots\; 0 \quad \cdots \quad 0 \;\vdots\; 0 \quad \cdots \quad 0\right]^T. \tag{3.19c}$$

The eigen-solutions of this system will give the natural frequencies of the beam-WRCs system.

From the solution of Eq 3.19, the modal displacement, $\widetilde{q}_n$, are substituted back into Eq (3.1) to give the response of the beam and surfaces S_1 of the cells while the displacements $y_l(t)$ and $\theta_l(t)$ are substituted into Eq (3.5) to obtain the response of the WRCs' plate, i.e. surface S_2.

The response of the original beam without the cells is also required to compare the noise reduction performance of the WRC concept. This is easily obtained as

$$w(x,t) = \sum_{n=1}^{N} \Phi_n(x) q_n(t) \tag{3.20}$$

where $\Phi_n(x)$ is the mode shape given by Eq (3.2) with $\widetilde{m}_b$ replaced by m_b and the modal displacement is

$$q_n = \left(\omega_n^2 - \omega^2\right)^{-1} F\Phi_n\left(x_f\right)e^{i\omega t} \tag{3.21}$$

where ω_n is the natural frequency of the original beam given by Eq (3.4) with $\widetilde{m}_b$ replaced by m_b.

3.4 Acoustic Quantities

The noise reduction performance of the WRC concept is investigated by computing the source strength, sound pressure, sound power, and radiation efficiency. These acoustic quantities give insight into the physical mechanisms associated with the low frequency noise reductions of the treatment. Each one of the equations supplies different information about the volume velocity control approach.

The source strength was defined in Chapter 2.2 as the rate of fluid displaced by a radiating structure. Numerical integration is used to compute the source strength for the beam-WRC and for the subsequent plate-WRC models. This is accomplished by dividing the radiating surface area into a mesh layout of small areas, $\Delta x \Delta y$, defined by the N_x and N_y surface elements. Each grid point subsequently defines the velocity at that location of the radiating system. It should be noted that numerical integration is used to calculate all acoustic quantities unless otherwise noted. Thus, the source strength is defined as

$$Q_{ss} = \sum_{1}^{N_x} \sum_{1}^{N_y} \vec{v}(x_s, y_s) \Delta x \Delta y \tag{3.22}$$

where $\vec{v}(x_s, y_s)$is the normal velocity of the radiating surface at the $\vec{r}_s = (x_s, y_s)$coordinate with element area $\Delta x \Delta y$. The source strength, sometimes referred to as volume velocity, has a direct relationship to the method of low frequency noise control by the WRC as discussed in Chapter 2.2.

Assuming the surface of a structure is embedded in a baffle, the acoustic pressure radiated at a point defined by $(\vec{r} = r, \theta, \phi)$ in the sound field is easily computed using the Rayleigh's integral [33] as

$$p(r, \theta, \phi) = \int_0^{L_{by}} \int_0^{L_{bx}} \frac{ik\rho_o c e^{-ik\vec{R}}}{2\pi\vec{R}} \vec{v}(x_s, y_s) dx dy \tag{3.23}$$

where $R = |\vec{r} - \vec{r}_s|$ is the distance to the observation point from the source. These vectors are illustrated in Figure 3.2.

The far-field pressure as a measure of effectiveness becomes less relevant as the frequency increases because of the multiple pressure lobes that form over the radiating system. Thus, to evaluate the efficiency of the WRC as a noise control method, the total radiated sound

power is used as the principal metric. In this work, the acoustic power is obtained by integrating the sound pressure in the far-field [33]

$$\Pi = \frac{R^2}{2\rho_o c} \int_0^{\pi/2} \int_0^{2\pi} |p(r,\theta,\phi)|^2 \sin\theta d\theta d\phi \qquad R >> L_{bx} \tag{3.24}$$

This equation is simply the integration of the sound pressure over a hemisphere of radius R that is center at the source shown in Figure 3.2.

A secondary metric to determine the effectiveness of the WRC to reduce low frequency sound radiation is the change in radiation efficiency from the original structure. The radiation efficiency is defined as the ratio of the acoustic power radiated from the structure to the acoustic power radiated from a baffled piston of the same area vibrating with uniform amplitude equal to the average mean square normal surface velocity of the radiating structure at a frequency for which the piston circumference ($2\pi r_p$) is much larger the acoustic wavelength: $kr_p >> 1$. Thus, radiation efficiency is given as follows

$$\sigma = \frac{\Pi}{\rho c S \overline{\langle v_n^2 \rangle}} \tag{3.25}$$

where S is the structure surface area, $\overline{\langle v_n^2 \rangle}$ is the spatial average mean square velocity of the structure, and ρc is the fluid impedance.

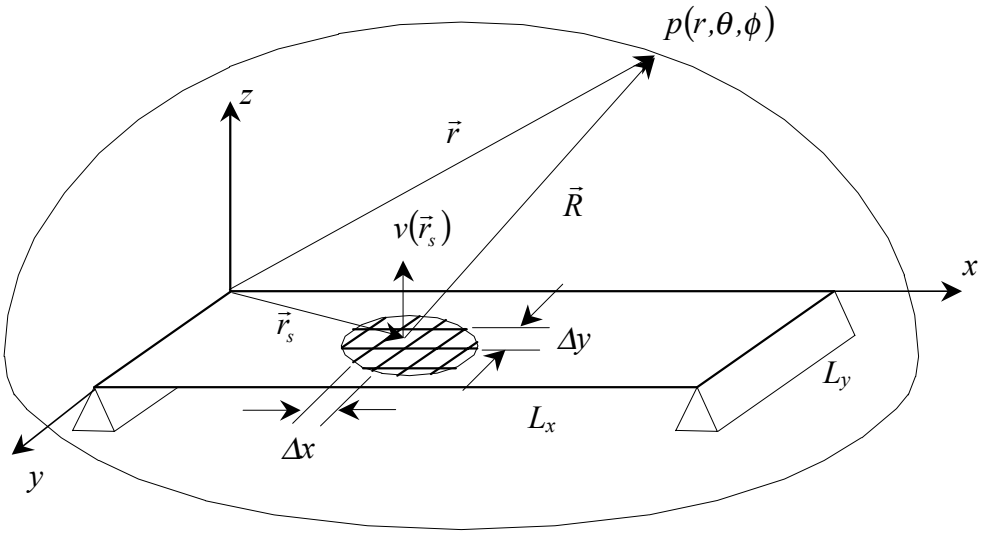

Figure 3.2: Schematic of beam in an infinite baffle with surface elements and hemisphere.

3.5 Numerical Analysis of the Weak Radiating Cell

The simplified model of the WRC presented in Chapter 2 was used to introduce the concept of the WRC and provide insight into the noise reduction mechanisms. Here, the model developed in the previous section is used to uncover additional physical noise reduction mechanisms associated to the WRC concept applied to a flexible structure. Results from this study suggest techniques to maximize the noise reduction capabilities of the WRC as well as minimize any negative effects produced by the WRC treatment.

In all the following case studies, unless otherwise noted, the simply supported beam has dimensions L_{bx} = 380 mm, L_{by} = 100 mm and thickness 4.5 mm and it is made of steel. A constant loss factor of 1%, *(η=0.01)* is applied to the modulus of elasticity E to account for structural damping i.e. $\hat{E} = E(1 + i\eta)$. The beam is driven with a point force of F = 1 N at x_f = 0.04 m. The frequency range investigated is 0–1600 Hz. In this range, the beam has four resonant modes occurring at 71.1, 284.4, 640.0, and 1137.8 Hz.

Four identical WRCs are applied to the beam to reduce the radiated noise. The surface area ratio is defined as $\mu = S_2/S_1$ and was selected such that $S_1 = S_2$, (i.e. μ = 1). This area ratio was chosen based on the initial work by Ross and Burdisso [27]. This study showed that the noise reduction performance of the WRC on a piston structure declines as the cell's plate surface S_2 is gradually made smaller than the cell's frame surface S_1. However, the study did not provide results for $S_2/S_1 > 1$. With area ratio equal to one, the dimensions of the cells are a = 67.2 mm, d = 70.7 mm, and e = .45 mm. As mentioned in the analytical section, the cell's frame masses are applied as a uniform distributed mass along the beam. Here, it is assumed that the total cell's frame masses is 15% of the beam total mass, i.e., $\tilde{m} = 1.15m$, which is similar to the values in the experimental work in reference 27. The cell's center plate has a mass M_l = 16.5 g, i.e. cell's plates represents 5% of the beam's

mass for a total mass ratio of 20%. The linear and rotational springs were selected such that the translational and rotational cell's resonances occur at 46 Hz $\left(\sqrt{k_l/M_l}/2\pi\right)$ and 58 Hz $\left(\sqrt{k_{tl}/J_l}/2\pi\right)$, respectively. In addition, the linear and rotation spring constants include a loss factors of 1%, $\hat{k}_l = k_l(1+i0.01)$ and $\hat{k}_{tl} = k_{tl}(1+i0.01)$. The parameters selected for the cells are such that the cells' dipole frequency (i.e., frequency of maximum volume velocity reduction) will be near the first resonance of the beam-WRCs system. The system described above is referred as the baseline case and will be used to investigate the noise reduction mechanisms. Table 3.1 summarizes the parameters used for the baseline beam-WRCs system. In addition, the impact of the addition of mass, damping, and the WRC's dynamics on the noise reduction performance are also studied.

Table 3.1: Physical parameters of the untreated beam and WRC(s)

	Steel Beam	WRC
Young's modulus (Pa)	195×10^9	—
Density (kg/m^3)	7700	—
Thickness (mm)	4.5	—
Dimensions (mm)	380×100	—
Beam Loss Factor, η	1%	—
Force Magnitude (N)	1	—
Forcing Location (mm)	40	—
Dimensions (mm), $S_1 = S_2$	—	67.2×70.7
Total Mass (kg)	1.3167	0.2633
WRC Loss Factor, η	—	1%

Figure 3.3 shows the driving point mobility at x = 0.04 m of the untreated beam and of the beam with the WRC installed. It should be noted that all frequency responses are normalized to the fundamental frequency of the beam f_n. To investigate the impact of the mass loading effect of the cells, Figure 3.3 also shows the driving point mobility of the beam with the cells' frames only. It is easily recognized from this figure that adding mass

(i.e., due to the cell's frames) to the beam lowers the resonant frequencies of the beam as well as leads to a small response reduction. The overall response of the beam both on and off resonance is decreased by 6.4% due to the additional mass. As expected, the decrease in beam response due to mass loading leads to a small reduction of sound radiated. The first resonance of the cells at 46 Hz and, less noticeable, the second resonance at 58 Hz are also evident in this figure as two small peaks. This occurs, because the cells' resonances are not close or tuned to any of the beam resonances, hence the dynamic interaction between the beam and cell's modes is insignificant. In addition, the weak coupling between the cells does not result in a noticeable shift in the cells' resonances i.e., less than a hertz. This is shown in Table 3.2, which provides the resonance frequencies of the linear and rotational mode of each WRC.

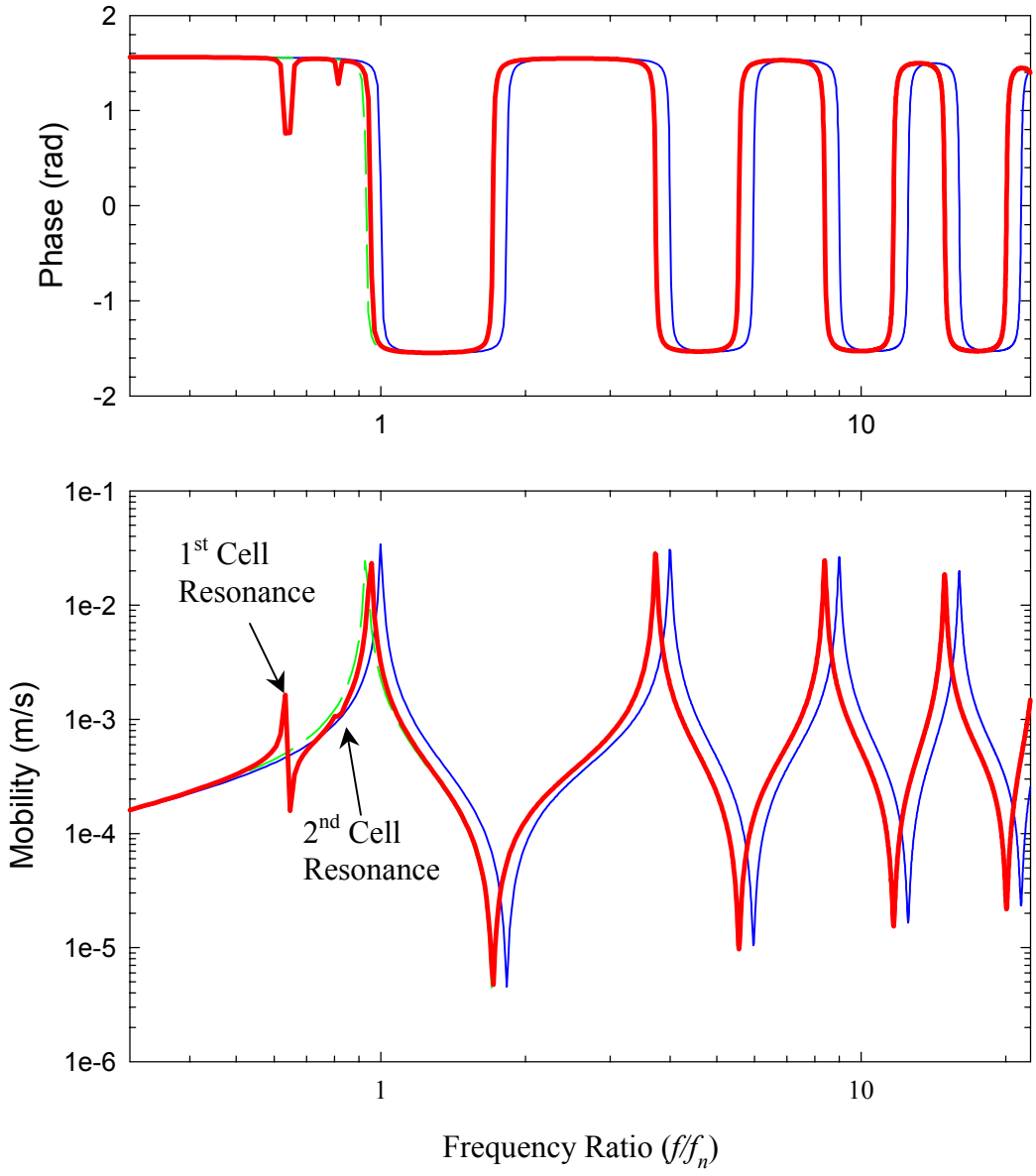

Figure 3.3: Driving point mobility of untreated beam (——) with four WRC (——); and the beam with the cells' frames (– – –).

Table 3.2: Global and Frequency Band Reductions (dB) with Frequency Perturbed Cell Resonances.

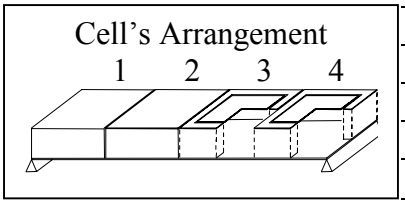

Cell (#)	Linear @ 46 (Hz)	Rotational @ 58 (Hz)
1	45.121	57.929
2	45.128	57.914
3	45.133	57.929
4	45.135	57.923

For the cells to behave as acoustic dipoles sources the cells' two surfaces, S_1 and S_2, relative motion must be out-of-phase and have equal amplitude. The response of the cells as acoustic dipoles is one of the fundamental mechanisms of the concept of volume velocity noise control. The results in Figures 3.4 through 3.6 are used to investigate the noise control mechanisms associated to the WRCs. Figure 3.4 shows the linear mobility response of the treated beam, at x = 0.2375 m and the third WRC's plate response $y_3(t)$, i.e., the calculated response is at the attachment point of the third WRC's spring. Figures 3.5a-d illustrate the response of the treated beam system at several key frequencies. Figure 3.6 shows the volume velocity of the original and the beam with WRCs as a function of frequency.

Comparison of both magnitude and phase in Figure 3.4 reveals that before the first WRC resonance the two surfaces are in phase. Moreover, as the frequency approaches the cells' first resonance at 46 Hz, the motion of the inner surface S_2 rapidly increases due to the dynamic amplification. This is illustrated in Figure 3.5a and it is evident that this yields a significant increase in volume velocity as shown by the peak at 46 Hz in Figure 3.6. This increase in volume velocity will result in an increase in the radiated power as compared to the untreated beam. Above the cell's first resonance, the two surface responses are now out-of-phase and in particular they have nearly equal magnitude around the cell's dipole frequency at f_d = 68 Hz. The phase shift leads to the behavior of the WRCs as acoustic dipoles. As seen in Figure 3.5b, around the dipole frequency the motion of the cell's two

surfaces, S_1 and S_2, of each WRC is out-of-phase. This response results in a dramatically sharp drop in volume velocity clearly seen in Figure 3.6. The volume velocity control mechanism in this frequency range, around the dipole frequency, is by motion modification (see Chapter 2 page 13).

The second resonance of the WRCs corresponds to the rocking motion of the cell. For the properties of the selected cells, it occurs before the dipole frequency at 58Hz (i.e., f/f_n = 0.82). The response of the WRCs in the rocking mode is shown in Figure 3.5c at the frequency of 285 Hz. Unlike the cell's fundamental resonance, the second resonance of the WRCs does not lead to sound increase because this mode is already an acoustic dipole source. However, it does not result in any additional noise sound reduction.

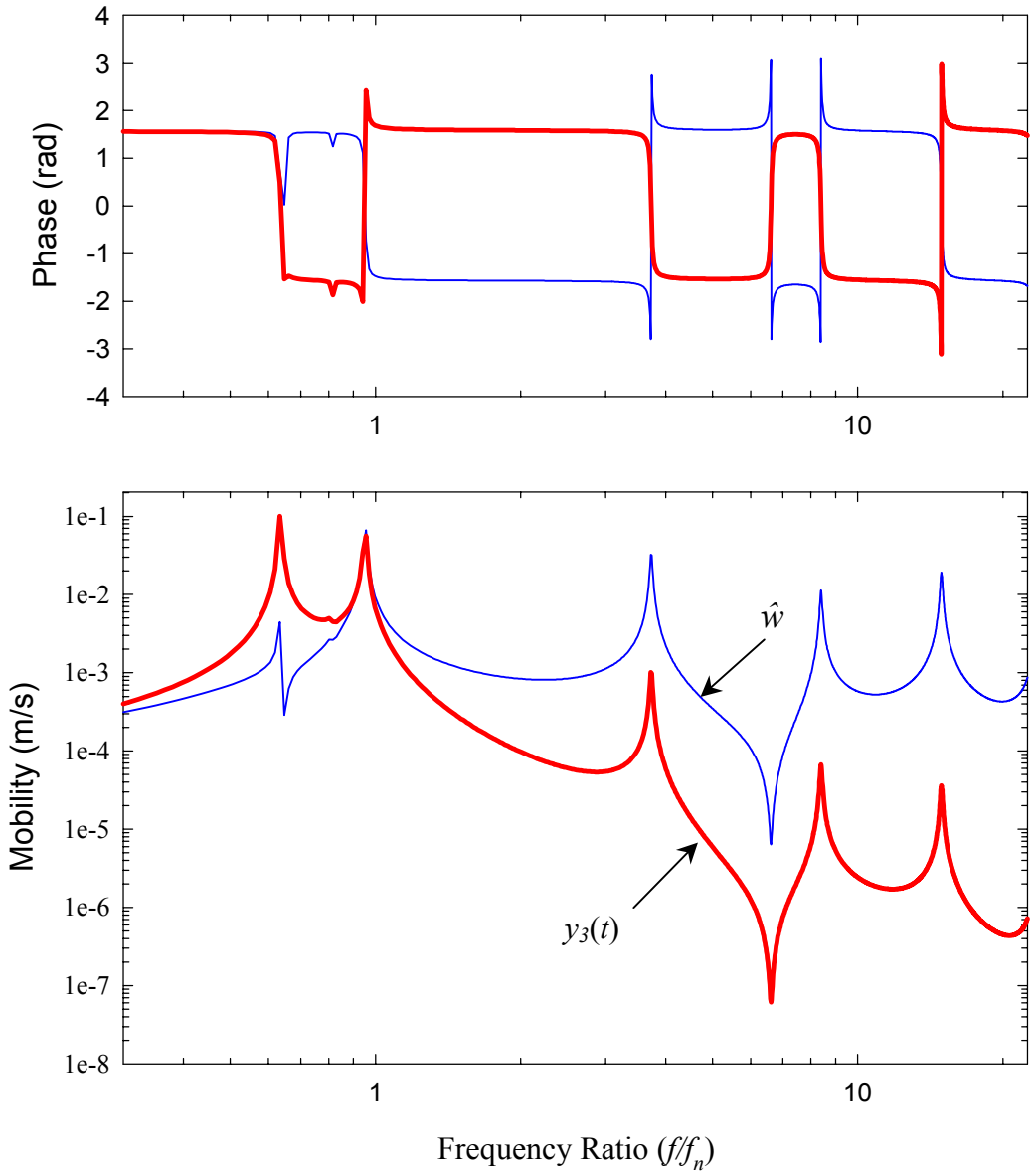

Figure 3.4: Mobility response of treated beam at $x = 0.2375$m: $\hat{w}(0.2375, t)$ (——) and of the third WRC's center plate, $y_3(t)$ (——).

As the frequency increases, the inner cell's surface S_2 becomes almost motionless because of the inertia of the center plate, see Figure 3.4. Note that the amplitude of the cell's $y_3(t)$ response is two order of magnitude smaller at frequencies $f \geq 6\, f_1$. Figure 3.5d illustrates this behavior. This brings forth the second noise reduction mechanism associated to the cells. At higher frequencies, noise reduction is achieved by suppression of the response of the cell's plate surface, S_2. For this particular case, effectively half of the radiating surface area has a response two order of magnitude smaller than the untreated structure. This lack of motion from the WRCs constitutes a reduction in volume velocity over a broad frequency range, thus making WRCs a broadband acoustic noise control method as shown in Figure 3.6.

Table 3.3: Peak Sound Power of Beam Configurations with Overall Reduction.

dB	Untreated	Mass Loaded	Treated
1st Beam Mode	86.0	82.4	53.7
2nd Beam Mode	80.5	79.0	71.6
3rd Beam Mode	81.2	79.9	72.2
4th Beam Mode	80.9	79.4	69.9
Overall Reduction (dB)		1.9	9.8

The most important metric to determine the effectiveness of the WRCs on the control of acoustic noise is sound power. The sound power gives a better perception of the noise reduction achievements while the source strength and frequency response calculations point out the physical mechanisms driving these reductions. Figure 3.7 shows the sound power spectrum of the untreated, treated and mass-loaded beam. Power level reductions at resonances as well as the overall sound level reduction are listed in Table 3.3. As pointed out in the previous section, the addition of mass results in a small reduction in the response of 6.4 % that leads to a constant reduction on the power spectrum of about 1.86 dB. Note

that this reduction will be smaller for lighter cells, which is desirable in some applications. Also shown in this figure, the sound power spectrum after the complete WRCs are implemented on the beam shows a power level reduction over the entire frequency range of interest, i.e. both on and off resonance frequencies, except at the cells' 1^{st} resonances. It is important to remark that in the higher frequency region the second noise control mechanism, suppression of the cell's center plate, constitutes a majority of the noise reduction. With cells' plates area representing 50 % of the total radiating area, it is estimated that 6 dB sound power level attenuation or a reduction of 4 times in the acoustic power should be achieved. A simple explanation to 6 dB of reduction is to consider two monopole sound sources radiating close to one another coherently, (i.e. the two cell surfaces S_1 and S_2). If S_1 generates an rms pressure P_{rms1} and S_2 generates an rms pressure P_{rms2}, the resultant total P_{rmst} pressure is $P^2_{rmst} = P^2_{rms1} + P^2_{rms2} + 2P_{rms1}P_{rms2}$ [30]. Since the sound power is proportional to P^2_{rmst} and assuming $P_{rms1} = P_{rms2}$, it results in a reduction of a factor of 4 when one of the two coherent monopole sources is eliminated i.e., the suppressed cell's plate area S_2.

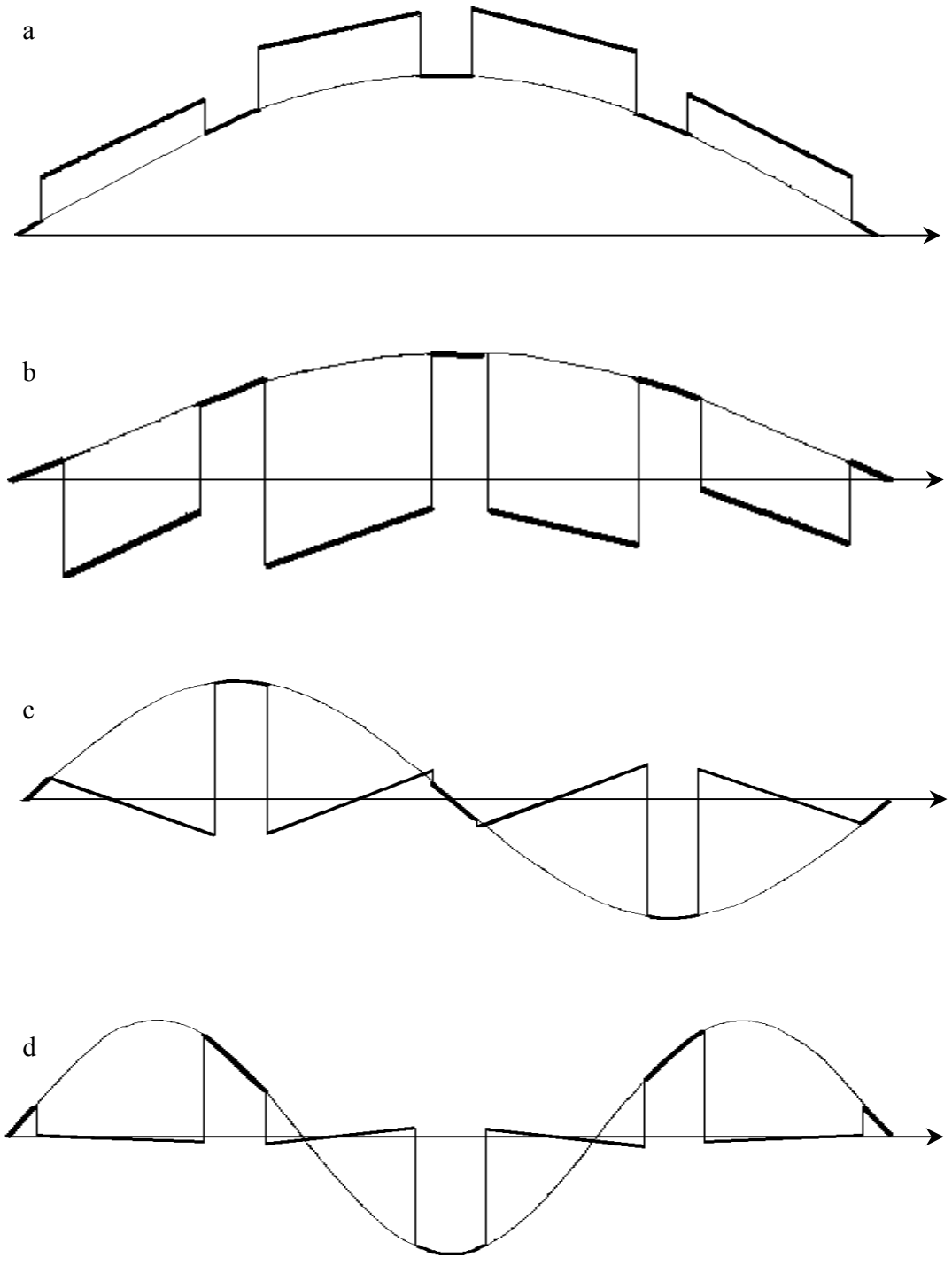

Figure 3.5: Response of the treated beam at (a) 30Hz, (b) 71 Hz, (c) 285 Hz, and (d) 640 Hz

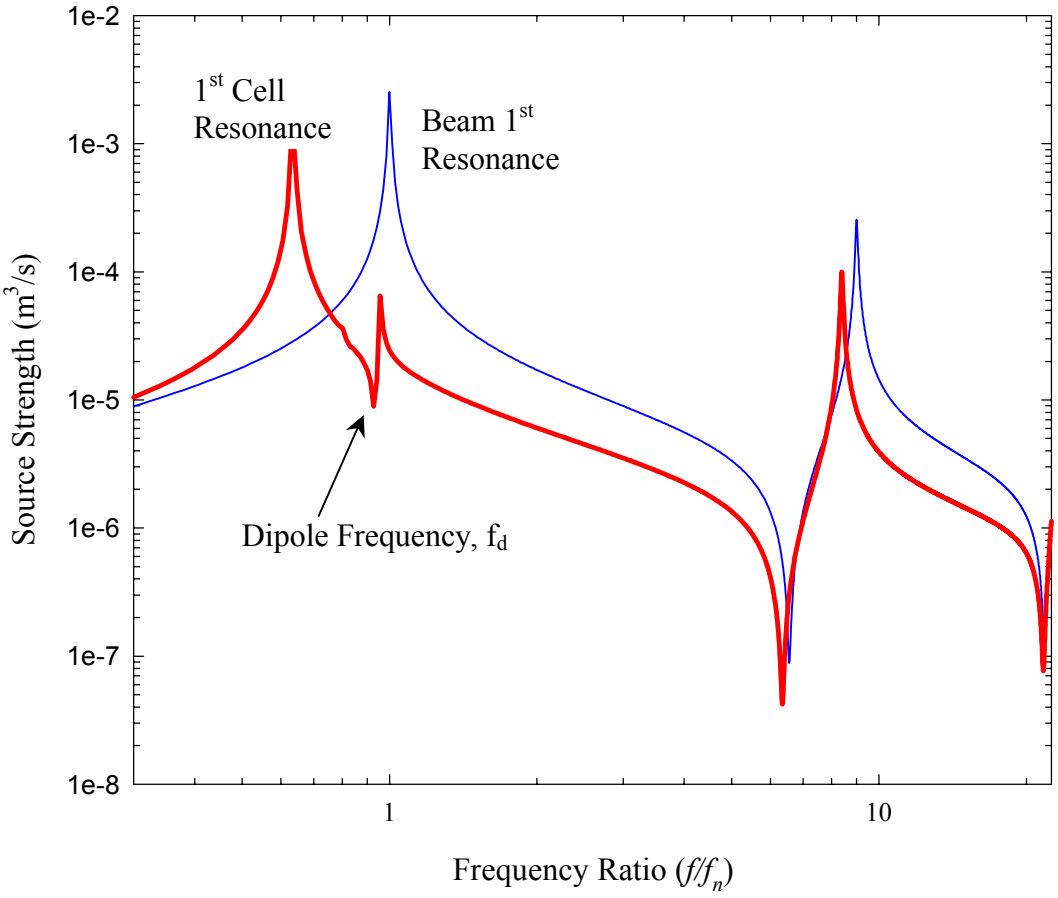

Figure 3.6: Volume Velocity of untreated (——) and treated beam (——).

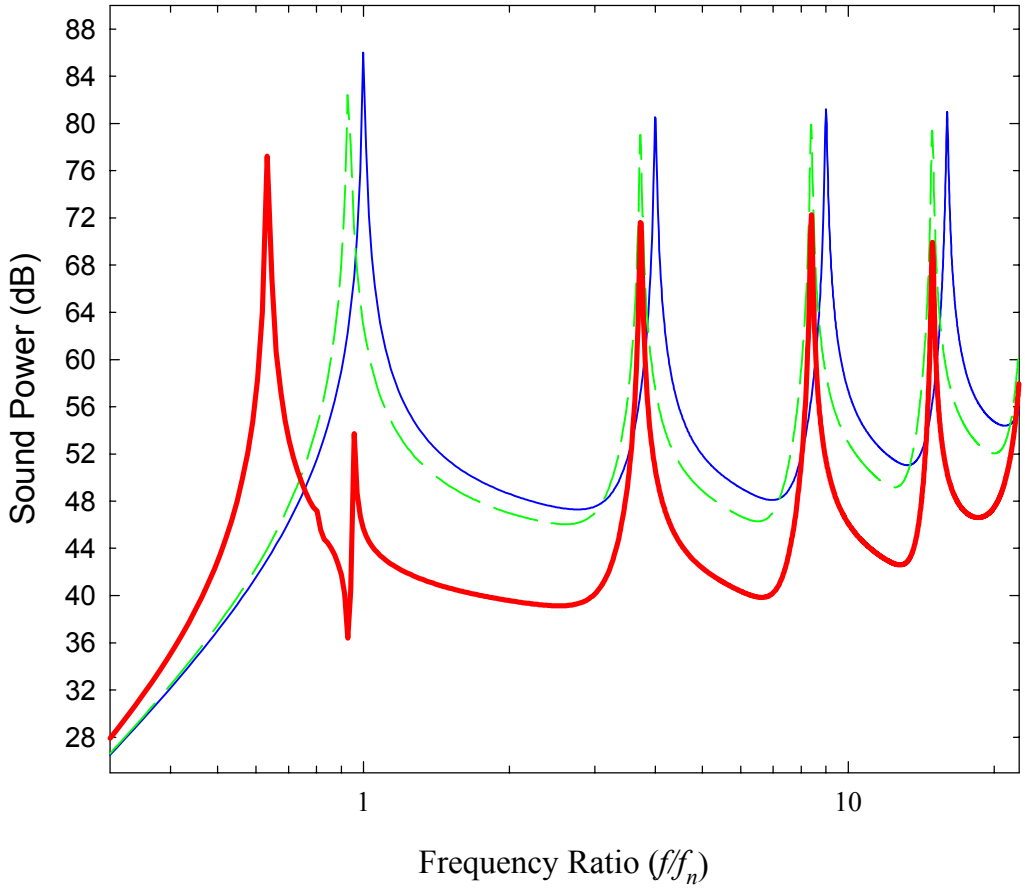

Figure 3.7: Sound power of untreated beam (——) with four WRC (——); and the beam with the cells' frames (– – – –).

Results in Figure 3.7 shows reductions near 8 dB for off resonance and near 10 dB at on resonance at higher frequencies, i.e., 1.86 dB due to mass loading plus 6 dB due to suppression of the center plates S_2. Finally, the full application of the WRCs accounts for 83.17% of the overall sound power reduction with an attenuation of 9.8 dB as compared to the untreated beam, i.e., all effects considered (see Table 3.4.)

For the case of a tonal disturbance, the design of the WRC should be such that the dipole frequency, f_d, of the cell is tuned directly around the disturbance frequency, which leads to maximum noise reduction. The tuning of the cell's dipole frequency to a dominant noise component of the noise spectrum is illustrated in Figure 3.8a-c. In these figures, the resonance frequency of the cells is set at 46 Hz while the dipole frequency is adjusted by changing the area ratio, $\mu = S_2/S_1$. Thus, the dipole frequency is then set to occur directly below, approximately at, and above the beam's first resonance. The results in Figure 3.8a-c show that reduction of up to 60 dB can be achieved at single frequency.

Finally, radiation efficiency is used to determine the efficiency of the structural response to couple with the acoustic medium. Figure 3.10 compares radiation efficiency results of the untreated beam and treated beam with the baseline WRCs. It is evident that the WRCs have an overwhelming reduction on the structure's ability to radiate sound to the far-field at the dipole frequency. It is also interesting to note that the rocking mode of the WRC reduces the efficiency of the beam although this is not apparent in the source strength in Figure 3.6. However, the rocking motion of the WRC is not the primary interest of the noise control mechanism. It is interesting to point out that the radiation efficiency is reduced nearly by half at higher frequencies, due to the suppressed radiating surface area S_2. It must be kept in mind that the reference average mean square normal velocity of the baffled piston is nearly reduced by 2. The oscillation of the radiation efficiency at higher frequencies is explained by interferences in pressure near the edges of the radiating structure. This topic is beyond the scope of this thesis, however work by Skudrzyk [30] covers edge waves effects.

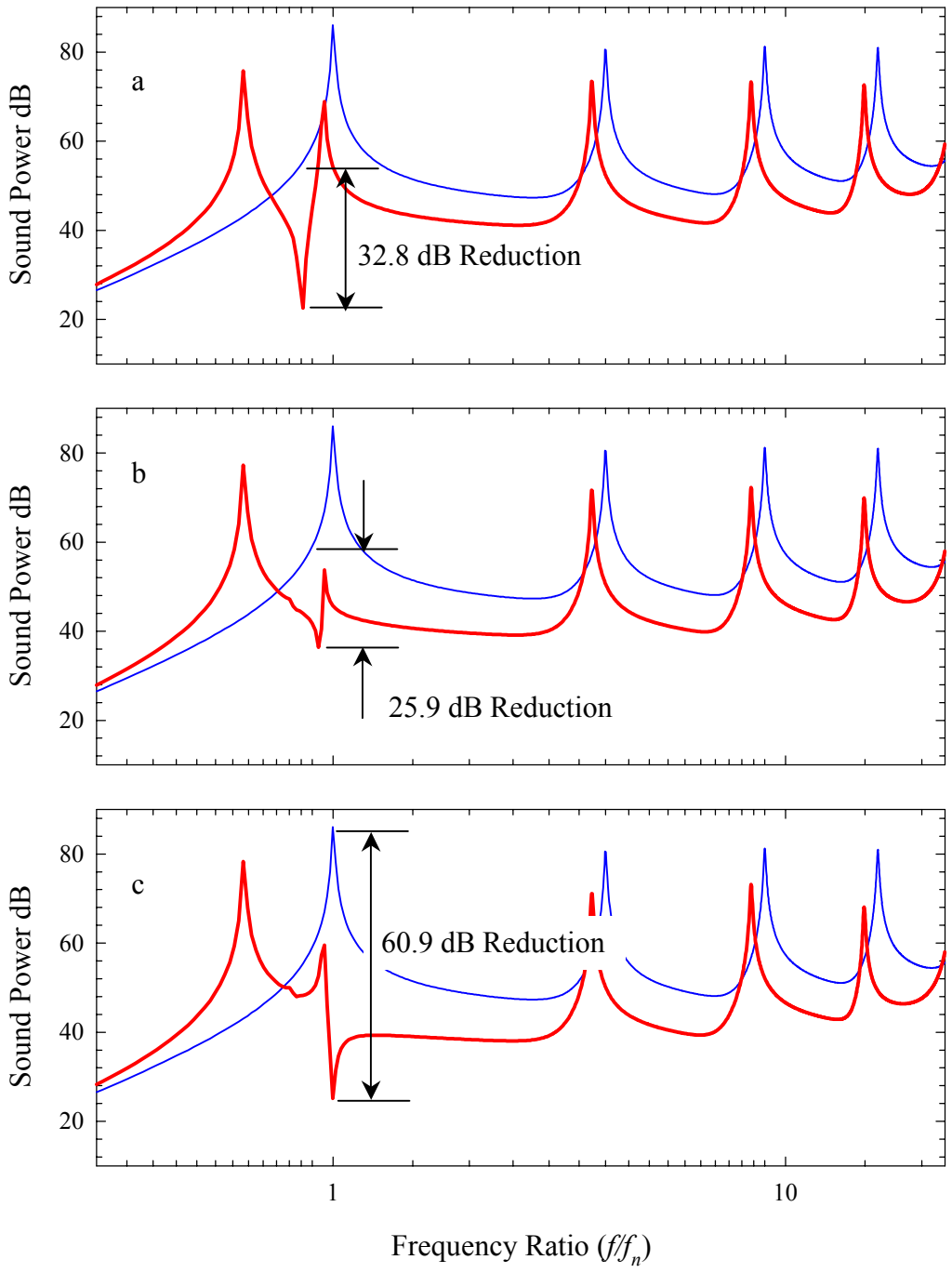

Figure 3.8: Tuning dipole frequency, f_d, to equal beam 1st natural resonance, f_n, by area ratio a) $\mu = .66$ b) $\mu = 1$ c) $\mu = 1.5$. Untreated (——) and treated (——) beam.

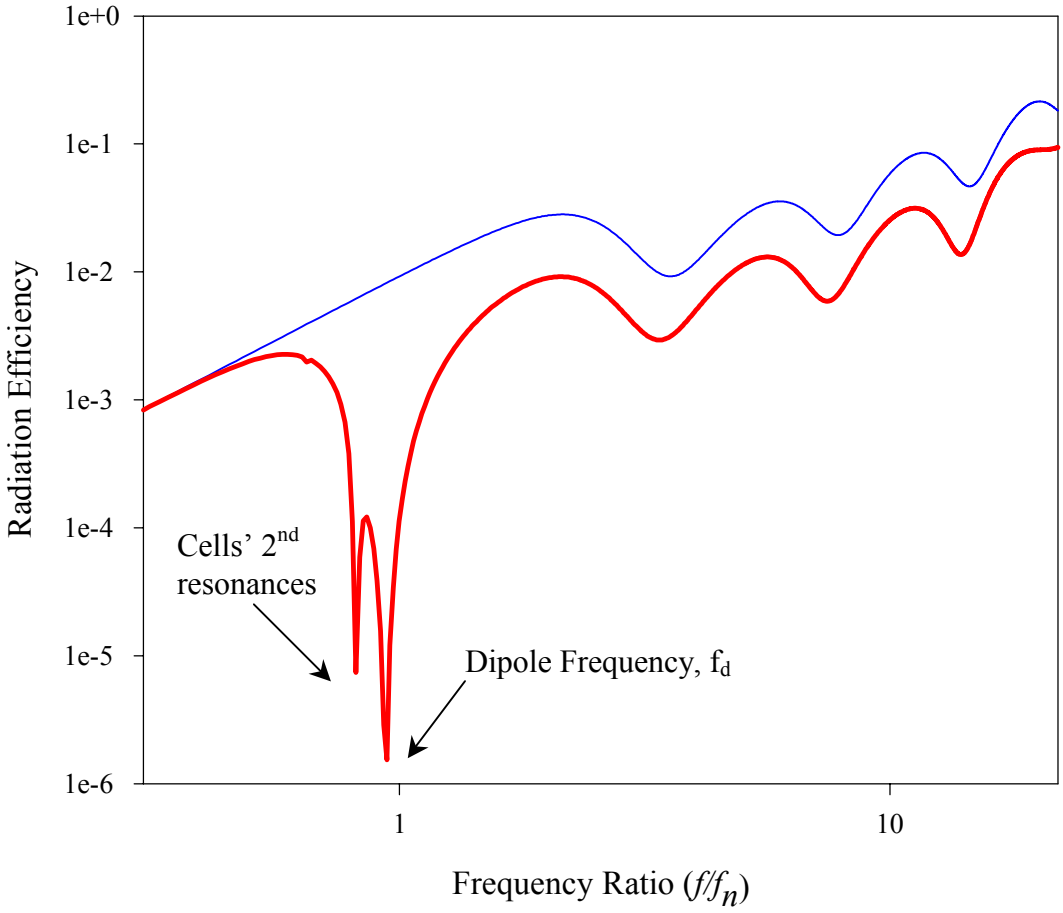

Figure 3.9: Radiation efficiency of untreated (——) and treated beam (——).

3.6 Methods to Improve Performance at WRC's Fundamental Resonance

As shown in the previous results, a drawback of the WRC is the noise increase associated to the cell's fundamental resonance, i.e., translational motion $y(t)$. This adverse effect of the WRC is alleviated if we considered A-weighted sound spectrum. This is illustrated in Figures 3.10, which shows the A-weighted sound power spectrum for the untreated and treated (baseline case) beams. The spectrum at 46 Hz (cell resonance) is corrected by -31.4 dB as compared to the –24.3 dB correction at 71 Hz or the beam 1st resonance. The difference in the correction makes the increase in noise at the cell's resonance somewhat less critical. This is evident when comparing the overall power reduction of 10.3 dB obtained from the A-weighted spectrum to the 9.8 dB reduction from the un-weighted spectrums in Figure 3.7. However, it is important to investigate options to further improve the performance of the cell by alleviating or suppressing the increased noise at the cell's resonance.

Placing the cell's resonance frequency outside that of the disturbance frequency is an obvious approach. This method works well when the disturbance is tonal or narrow band. Increasing the damping of the cells to reduce the cell's resonance response is also an obvious approach. Another potential solution is to add a perturbation to the properties of the WRCs such that they have different resonance frequencies. In this way, the adverse effect of all cells resonating at the same frequency is potentially alleviated. Here, several studies are presented to investigate the effectiveness of these two approaches.

Active control can also be a very effective approach to suppress the resonance of the cell and the increase in noise. However, the main focus here is to investigate purely passive methods. The implementation of active control is beyond the scope of the present work.

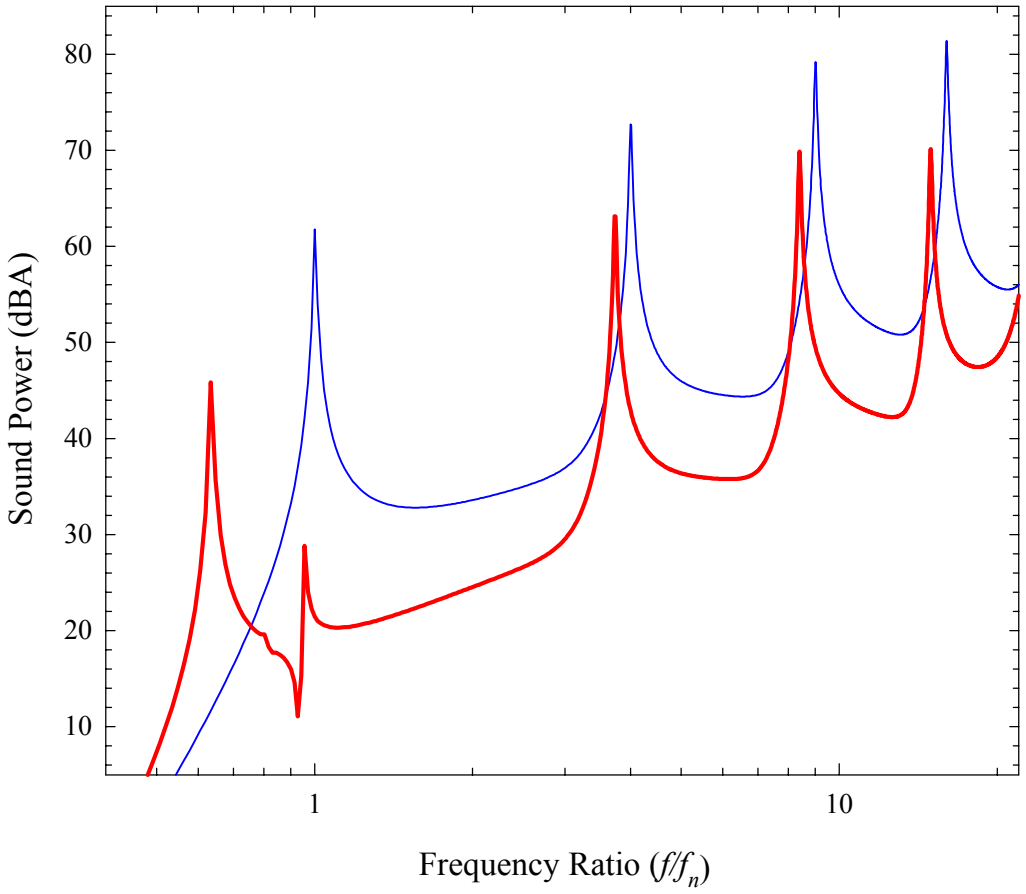

Figure 3.10: A-Weighted Sound Power Spectrum of untreated (——) and treated beam (——).

3.6.1 Addition of Damping to WRC

One method of minimizing the noise created by the WRC treatment is adding damping to the translation springs. To maintain consistency, identical damping values were added to the rotational spring as well. Using the same set of parameters for the beam and the WRC given in Section 3.5 several different loss factor values are applied to the springs of the WRC. Figure 3.11 shows the sound power spectrum for the treated beam with several loss factors applied as well as the untreated beam. As expected, increasing the energy dissipation in the cells' springs decreases the response of the cell's plate at resonance. However a decrease in the noise reduction at the dipole frequency is also observed. This is due to the two surfaces being less out-of-phase, which shifts the cell's dipole frequency as well as lowers the cell's resonance response.

Table 3.4: Global and Frequency Band Reductions (dB) for Cell Damping Implementation.

Loss Factors	1%	2%	6%	9%	12%	15%	24%	27%	50%
Reduction (dB) 0-251 Hz	9.0	13.2	18.6	19.6	20.0	20.0	19.4	19.1	17.0

To quantify these effects, Table 3.4 gives the global noise reduction determined for the various damping cases in the frequency range of 0-250 Hz. In this frequency range, the effect of the additional damping is very apparent. From the table, an additional sound power reduction of 11 dB occurs when the loss factor is increase from 1 to 12%, which is a substantial improvement in the performance of the cell. However, Table 3.4 also shows that an optimum value of damping exists for a specific tuned dipole frequency.

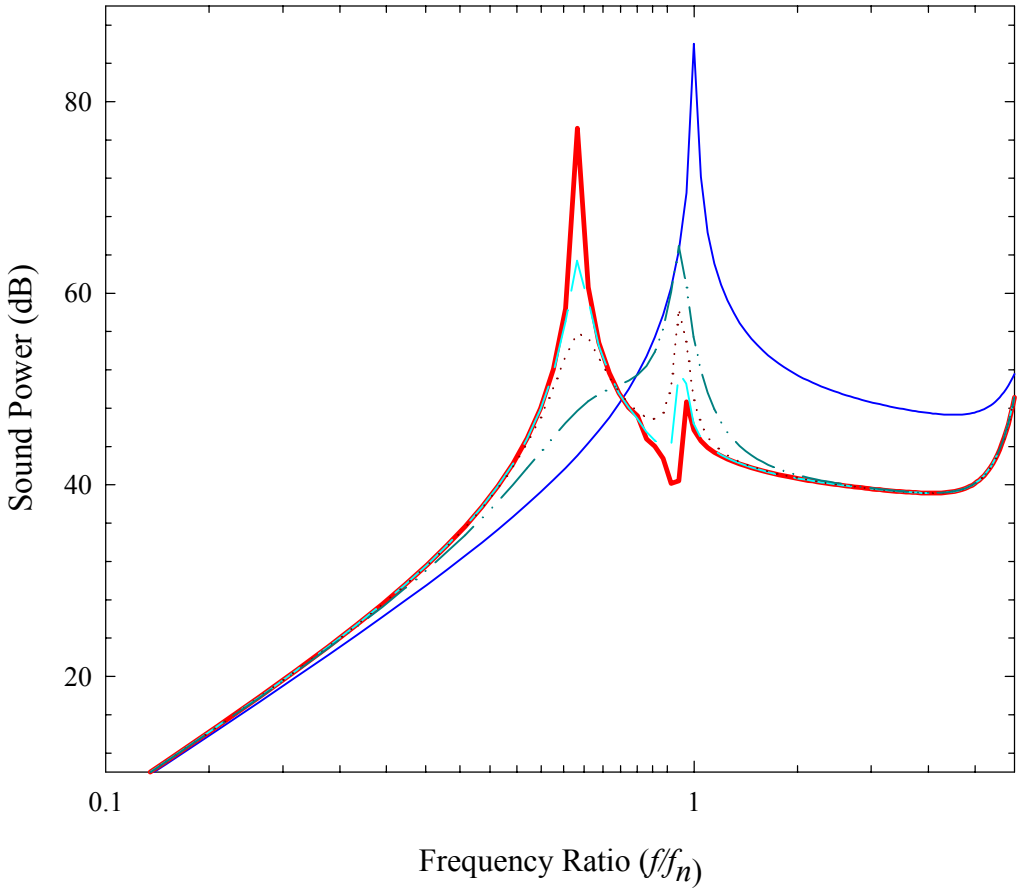

Figure 3.11: Spectral results of damping implementation in cells; untreated beam (——), η = 1% (——), η = 6% (– – –), η = 15% (·····), η = 50% (–·–·–)

3.6.2 WRC Resonance Frequency Perturbation

The second approach to alleviate noise created by the cells at resonance is to adjust each cell's resonance to occur at a slightly different frequency. The effect of separating the resonance frequencies of each cell causes the collective noise created at the mean resonance frequency to decrease. In this study, the cells' resonance frequencies for the four WRCs are adjusted by changing their spring constants. Several perturbation cases were investigated. These cases are described in Table 3.5, which shows the translational frequency of each cell for each case investigated. However, the mean translational resonance frequency of the WRCs is kept at 46 Hz for all cases. The rotational resonance frequency of each WRC is also held at 58 Hz.

Table 3.5: Global and Frequency Band Reductions (dB) with Frequency Perturbed Cell Resonances.

Cell's Arrangement	Case #	Cell's Frequency (Hz)	Standard Deviation	Reduction (dB) 0 –251 Hz
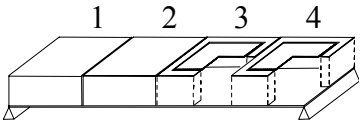	Baseline	46 46 46 46	0.0	9.37
	1	44 45 47 48	1.58	16.9
	2	43 45 47 49	2.23	15.9
	3	43 44 48 49	2.55	16.7
	4	42 44 48 50	3.16	19.7
	5	42 43 49 50	3.53	17.3
	6	41 43 49 51	4.12	16.2
	7	41 42 50 51	4.52	15.7

To help better illustrate this concept, Figure 3.12 shows the 1st and 3th cells' linear mobility response for the fourth case of Table 3.5. As seen in the figure, the 1st cell has resonance at 42 Hz (f/f_n = 0.59) while the 3rd cell has a resonance at 48 Hz (f/f_n = 0.68). It is observed that their motion is out-of-phase between those frequencies. Additionally, Figure 3.13 illustrates the motion of the WRC-beam system at 45 Hz where the two cells' motion is nearly the same. Notice that the 1st and 2nd cells' plates are below the beam operating out-

of-phase with 3rd and 4th cells' plates. Also note that the 2nd cell's plate translation response is highly excited i.e., close to resonance. Another observation in Figure 3.12 is the responses of the cells' plates do not stay in phase throughout the frequency range of interest. However this does not contribute to noise control at higher frequencies where cells' plate motion is small as compared to the beam.

To demonstrate how the perturbed cells' resonances help minimize the noise, Figure 3.14 shows the sound power spectrum for the untreated beam, and the perturbed case treated beam for 0–251 Hz. The heavy line represents the 4th case of Table 3.5 when the four WRCs have translation resonant frequencies at 42, 44, 48 and 50 Hz, respectively. As expected, the noise associated with the perturbed WRCs is minimized with the sound power distributed over a wider frequency band. Also, the reduction at the dipole frequency has only increased by 3 dB as compared to the results presented in Figure 3.7. As seen previously by the other method of controlling WRC noise at

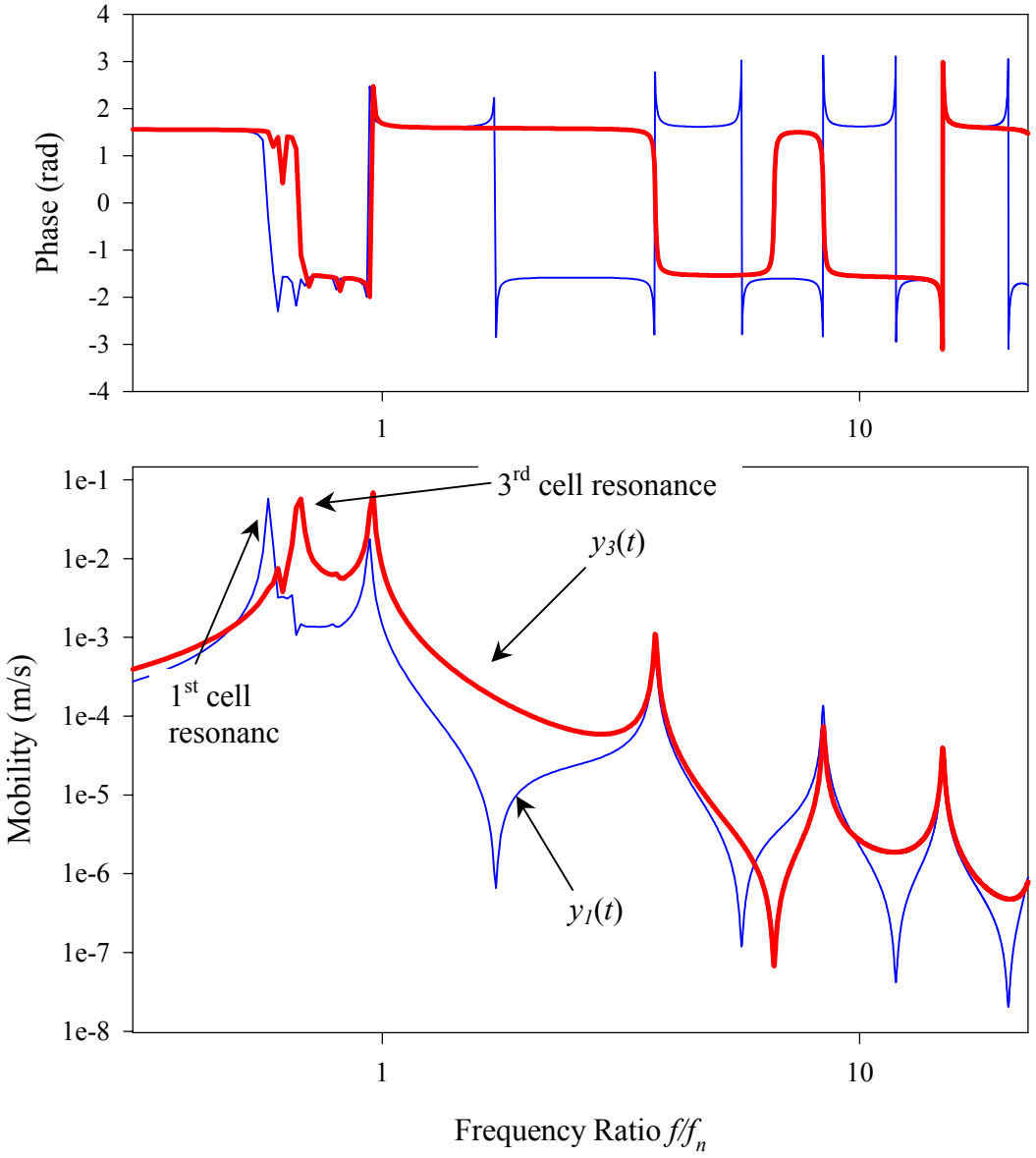

Figure 3.12: Mobility response of the 1st WRC's center plate (——) and the 3rd WRC's center plate (——).

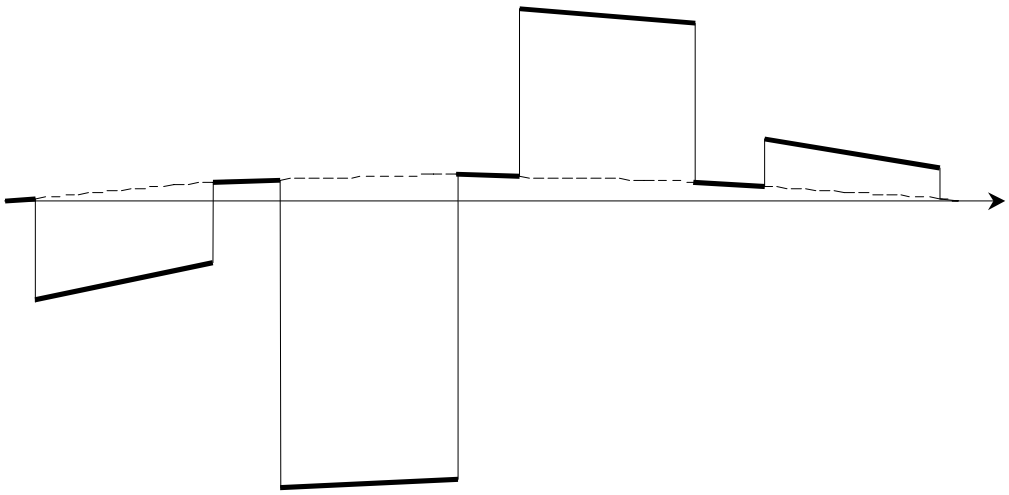

Figure 3.13: Illustration of WRC-beam response with perturbed WRC resonant frequencies at 45 Hz

resonance, the perturbation results found in Table 3.5 indicates a maximum possible noise reduction. Once the separation of the resonance frequencies is extensive the noise control method becomes detrimental, resulting in increased noise by the WRCs again.

To further illustrate this perturbation method, Figure 3.14 also shows the results if all four cells resonate at a single frequency. The thin lines are the sound power levels if all four WRCs are tuned to the same translation resonant frequency relative to each perturbed frequency of the fourth case. From the figure it is possible to see the resonance of the tuned WRCs and their respective dipole frequency, f_d. Notice as the frequency approaches the second cell's resonance, the first cell has passed resonance and is now operating out-of-phase. This creates a local dipole between the two WRCs lowering the noise radiated of the second cell. Although, a neighboring cell cannot alleviate the noise created by the 1st WRC, the beam disturbance is far enough that the cell fundamental resonance is not amplified.

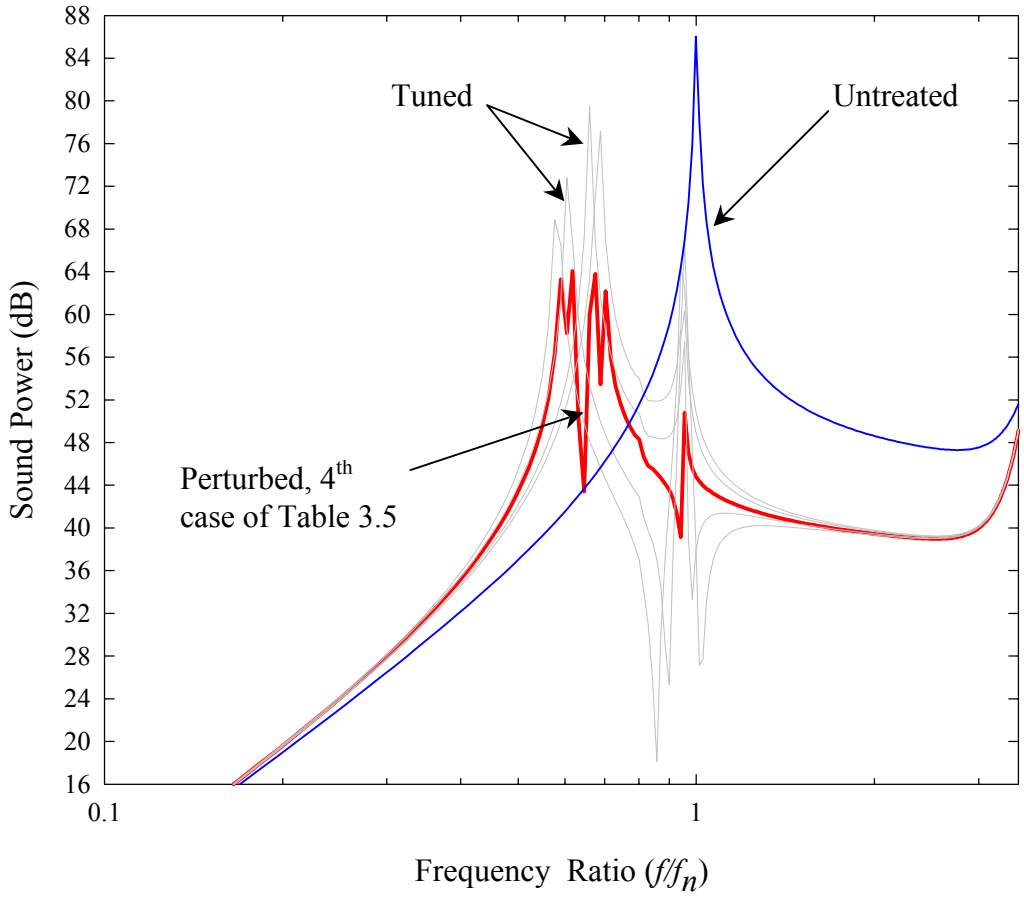

Figure 3.14: Spectral results of perturbation in cell resonance frequencies; untreated beam (——), tuned cells (——), and perturbed cells (——).

3.6.3 Resonance Frequency Perturbation and Addition of Damping, η

Previously it was shown that perturbation in the translational resonant frequencies of the WRCs provided one method of improving noise control at WRC resonance. The other method introduced damping into the flexible medium (i.e., the cells' springs), which dissipated energy and minimized sound increase associated with the WRC resonance. For both methods, an optima level of noise attenuation was shown to exist. Here a parametric investigation of the combination of these methods is considered.

This study uses a combination of the addition of damping and perturbed resonant frequencies provided in Tables 3.3 and 3.4. Figure 3.15 shows the sound power reduction results in the 0–251 Hz frequency range as a function of the loss factor and perturbation case. It is seen in the figure that perturbation of the resonant frequencies has a significant effect on noise reduction when the damping of the WRC is small (i.e., $\eta < 3$). As the damping increases, results indicate slight added benefit with only a 1dB increase in noise reduction as seen in the perturbation case 6. The addition of damping shows a similar trend as seen in Section 3.6.1. However, the optimum damping of a 9% loss factor provides the optimal sound reduction with perturbation. Again the noise reduction roll-off is associated to the relative phase shift and suppressed motion of the WRC due to excessive damping.

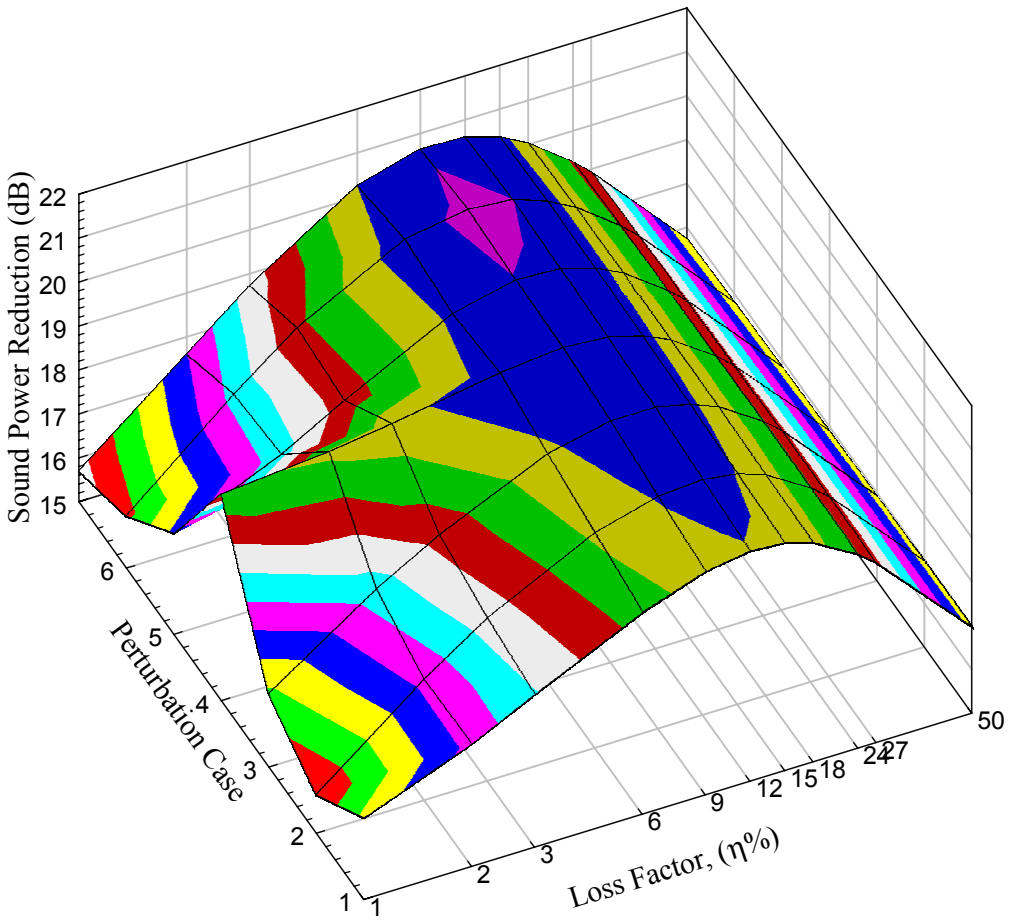

Figure 3.15: Sound power reduction of frequency 0–251 Hz for perturbation and loss factor parametric study of WRCs

3.7 Wavenumber Transform Analysis

Another approach to interpret the noise reduction mechanisms of the WRCs is to use a wavenumber transform analysis. This method of analysis associates sound energy from individual wavenumber components of the normal velocity distribution of any planer structure in an infinite baffle. Figure 3.16 illustrates a transverse-structural bending wave of frequency ω and wavenumber vector k_b traveling along the positive x direction. To satisfy the boundary conditions at the structure-fluid interface $y = 0$, the x-component of the acoustic wavenumber vector, k_x, has to match the structural wavenumber i.e., $k_x = k_b$. [34]. The y-component of the acoustic wavenumber vector, k_y, determines the sound generation characteristic of the structural wave. Thus, the acoustic wavenumber $k_o = \omega/c$ is related to k_x and k_y as $k_o = \sqrt{k_x^2 + k_y^2}$.

Thus, three distinct acoustic wavenumber cases can occur depending on the wave speed, c_p, in the structure. The wavenumber components termed supersonic occur when the structural wavenumber is less than the acoustic wavenumber, $k_b < k_o$, (i.e., the structure's wave phase speed is greater than the speed of sound in the fluid $c_p > c$). In this case, plane waves travel away from the structure surface at angle to the normal given as $cos\phi = k_y/k_o$ and $k_y = \sqrt{k_o^2 - k_x^2}$.

Subsonic wavenumber components are defined when the structural wavenumber is greater than the acoustic wavenumber, $k_b > k_o$, (i.e., the structure's wave phase speed is less than the speed of sound in the fluid $c_p < c$). In this case, the wavenumber component, k_y, of the acoustic wavenumber is imaginary such that $k_y = -j\sqrt{k_b^2 - k_o^2}$. Thus, sound pressure waves decay exponential with distance normal to the surface and the sound waves are called evanescent waves.

The last case occurs when the structural wavenumber equal the acoustic wavenumber $k_b = k_o$ which define the critical frequency. This case indicates that for a finite vibration of the structure infinite pressure occurs, which can never physically occur in the real world [35].

From the discussion above, wavenumber transform analysis of the beam velocity will prove useful in studying the behavior of the beam with WRC(s) applied as treatment. To this end, we make use of the wavenumber transform given as

$$V(k_x) = \int_{-\infty}^{\infty} v(x) e^{jk_x x} dx \tag{3.26}$$

which converts spatial-dependent velocity response into the wavenumber domain. The transform in Eq 3.26 indicates that the velocity response $v(x)e^{i\omega t}$ is expressed as the superposition of an infinite set of propagating waves with wavenumber k_x and amplitude $V(k_x)$. Thus, the normal centerline surface velocity distribution of the beam-WRCs system can be transformed for wavenumber analysis of the subsonic and supersonic waves. To this end, Figure 3.17 illustrates a simply supported beam with N_c WRCs. The normal surface velocity response of the beam-WRC system can be written as

$$\begin{aligned} v(x,t) = i\omega \sum_{n=1}^{N} \tilde{\Phi}_n(x) \tilde{q}_n(t) \qquad & \{H[x] - H[x - L_{bx}]\} \\ + i\omega \sum_{l}^{N_c} \left[(y_l(t) + \theta_l(t)) - \sum_{n=1}^{N} \tilde{\Phi}_n(x_l) \tilde{q}_n(t) \right] \quad & \left\{ H\left[x - \left(x_l - \frac{a_l}{2} \right) \right] - H\left[x - \left(x_l + \frac{a_l}{2} \right) \right] \right\} \end{aligned} \tag{3.27}$$

where $\tilde{\Phi}_n(x)$ is the normalized mode shape, Eq 3.2, $y_l(t)$ and $\theta_l(t)$ define the translation and rotational responses of the WRC, and H is the Heavyside operator [36] defining the piecewise velocity distribution of the surfaces, S_2 and S_1. Recall that the surface response of S_2 is considered to be the same as the beam response. Substituting Eq 3.27 into Eq 3.26 gives

$$V(k_x)=\int_0^{L_{bx}} j\omega\sum_{n=1}^{\mathrm{N}}\tilde{\Phi}_n(x)\tilde{q}_n(\omega)e^{jk_x x}dx+$$
$$\sum_l^{N_c}\left[\int_{(x_l-a_l/2)}^{(x_l+a_l/2)} j\omega\left\{y_l(\omega)+(x-x_l)\theta_l(\omega)-\sum_{n=1}^{\mathrm{N}}\tilde{\Phi}_n(x)\tilde{q}_n(\omega)\right\}e^{jk_x x}dx\right] \tag{3.28}$$

The various integrals in Eq 3.27 con now be solved as follows

$$V_1(k_x)=\int_0^{L_{bx}} j\omega\sum_{n=1}^{N}\tilde{\Phi}(k_x)\tilde{q}_n(\omega)e^{jk_x x}dx$$
$$=j\omega\sum_{n=1}^{N}\tilde{q}_n(\omega)\sqrt{\frac{2}{\tilde{m}L_{bx}}}\frac{\left(\frac{n\pi}{L_{bx}}\right)\left[(-1)^n e^{jk_x L_{bx}}-1\right]}{k_x^2-\left(\frac{n\pi}{L_{bx}}\right)^2}\quad ; \qquad -\infty\le k_x\le\infty \tag{3.29}$$

$$V_2(k_x)=\sum_l^{N_c}\left[\int_{(x_l-a_l/2)}^{(x_l+a_l/2)} j\omega y_l(\omega)e^{jk_x x}dx\right]=\sum_l^{N_c}\frac{2j\omega y_l(\omega)}{k_x}sin(k_x x_l)e^{jk_x x_l}\ ; \tag{3.30}$$

$$V_3(k_x)=\sum_l^{N_c}\left[\int_{(x_l-a_l/2)}^{(x_l+a_l/2)} j\omega\theta_l(\omega)e^{jk_x x_l}\right]=\sum_l^{N_c}\left\{\omega\theta_l(\omega)e^{jk_x x_l}\left[\frac{2x_l cos(k_x x_l)}{k_x}-\frac{2sin(k_x x_l)}{k_x^2}\right]\right\}$$

(3.31)

and

$$V_4(k_x)=-\sum_l^{N_c}\left[\int_{(x_l-a_l/2)}^{(x_l+a_l/2)} j\omega\sum_{n=1}^{N}\tilde{\Phi}_n(x_l)\tilde{q}_n(\omega)e^{jk_x x}dx\right]= \tag{3.32}$$

$$V_4(k_x)=-\sum_l^{N_c}\left\{\sum_{n=1}^{N} j\omega\tilde{q}_n(\omega)\sqrt{\frac{2}{\rho AL_{bx}}}\left[\frac{V^+-V^-}{\left(\frac{n\pi}{L_{bx}}\right)^2-k_x^2}\right]\right\}$$

where

$$V^{+} = e^{jk_x(x_l + a_l/2)}\left[(jk_x)sin\left(\frac{n\pi(x_l + a_l/2)}{L_{bx}}\right) - \left(\frac{n\pi}{L_{bx}}\right)cos\left(\frac{n\pi(x_l + a_l/2)}{L_{bx}}\right)\right]$$

$$V^{-} = e^{jk_x(x_l - a_l/2)}\left[(jk_x)sin\left(\frac{n\pi(x_l - a_l/2)}{L_{bx}}\right) - \left(\frac{n\pi}{L_{bx}}\right)cos\left(\frac{n\pi(x_l - a_l/2)}{L_{bx}}\right)\right].$$

Thus, the wavenumber transform is $V(k_x) = V_1(k_x) + V_2(k_x) + V_3(k_x) + V_4(k_x)$.

The wavenumber transform of the original beam without the cells is also required to compare the wavenumber modulus of the WRC concept. This is obtained as

$$\begin{aligned} V_b(k_x) &= \int_0^{L_{bx}} j\omega \sum_{n=1}^{N} \Phi(k_x) q_n(\omega) e^{jk_x x} dx \\ &= j\omega \sum_{n=1}^{N} q_n(\omega) \sqrt{\frac{2}{mL_{bx}}} \frac{\left(\frac{n\pi}{L_{bx}}\right)\left[(-1)^n e^{jk_x L_{bx}} - 1\right]}{k_x^2 - \left(\frac{n\pi}{L_{bx}}\right)^2} \qquad -\infty \le k_x \le \infty \end{aligned} \tag{3.33}$$

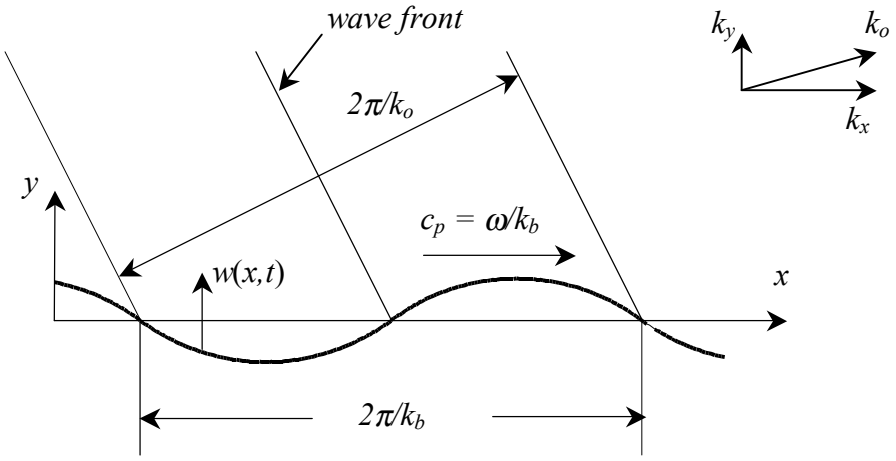

Figure 3.16: Travel wave in a infinite beam.

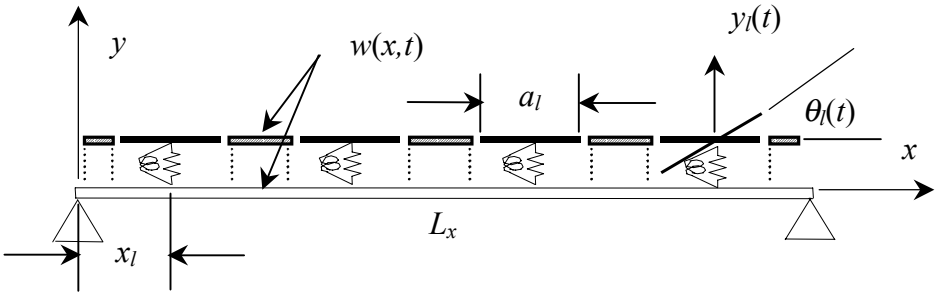

Figure 3.17: Model of WRC/beam response.

3.7.1 Wavenumber Numerical Results

The physical properties of the simply supported beam are the same used as the baseline case in the previous studies (see Table 3.1). The WRCs applied to the beam as treatment have physical properties of the specific set used in the perturbation study case four in Table 3.5.

Figures 3.18 and 3.19 plot the magnitude of the velocity wavenumber spectrum, $|V(k_x)|^2$ in dB [35], of the untreated and treated beam for the frequency range 0-1600 Hz. Figures 3.20 and 3.21 plot an exploded view of the dipole frequency region for frequencies 0–300 Hz. The dotted line separates the subsonic and supersonic regions. As expected, Figure 3.18 distinctly indicates spectral peaks when $k_x = n\pi/L_{bx}$ where the left half, k_x, equals the mode wavelength. It is important to note, when n = 1 (i.e., the beam's fundamental structural wavelength) an exception to the modulus spectrum occurs in that the maximum value happens at k_x = 0 (the dc value). Comparison of Figure 3.20 and Figure 3.21 illustrates an increase in supersonic and subsonic components of the wavenumber spectra near the WRCs resonant frequencies. In addition, the figures show that in the region of the dipole frequencies, near the beam's first resonance, the supersonic components are decreased, yet the subsonic components are increased. Recall that only the wavenumber spectra within the supersonic region contribute to the radiation of sound into the far-field, while the subsonic region only creates localized fluid disturbances near the two radiating surfaces. At higher frequencies, Figure 3.19, above the beam's first resonance and associated with the inertia effects of the WRC inner plate both the supersonic and subsonic components of the wavenumber spectra are decreased.

These results once again illustrate the effectiveness of the WRC method as an acoustic treatment for reducing low frequency far-field radiated noise. Another interesting

discovery resulting near the dipole frequency region was the increase in the subsonic wavenumber components leading to high fluid motion near the surface, not previously revealed by the previous acoustic results.

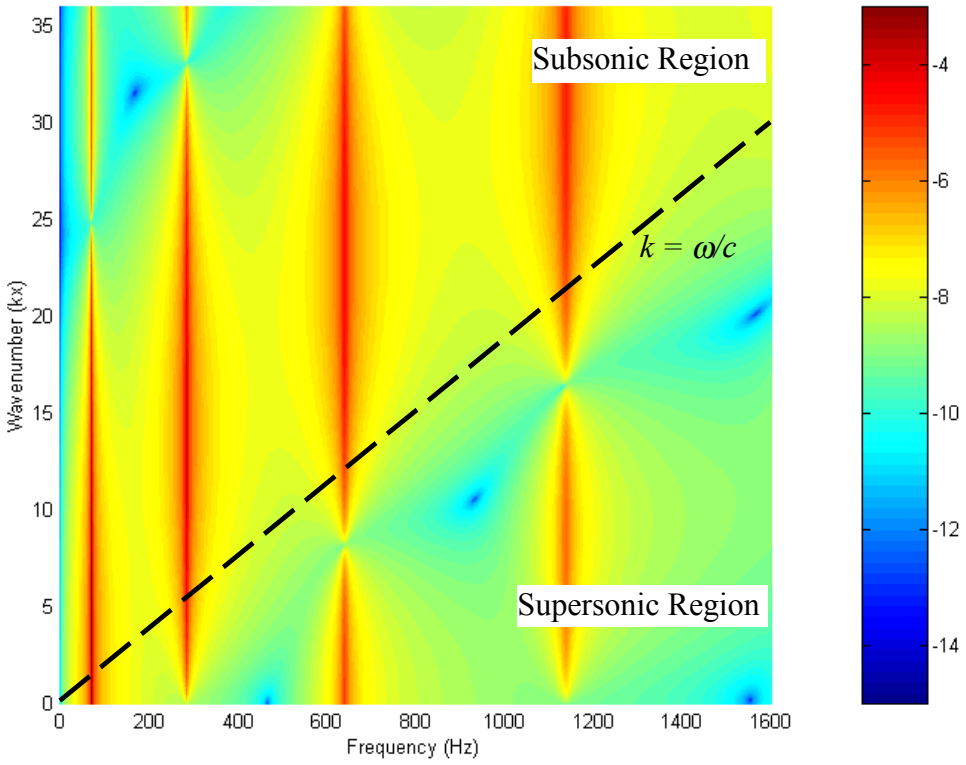

Figure 3.18: Wavenumber spectrum of untreated beam for frequency band 0–1600 Hz.

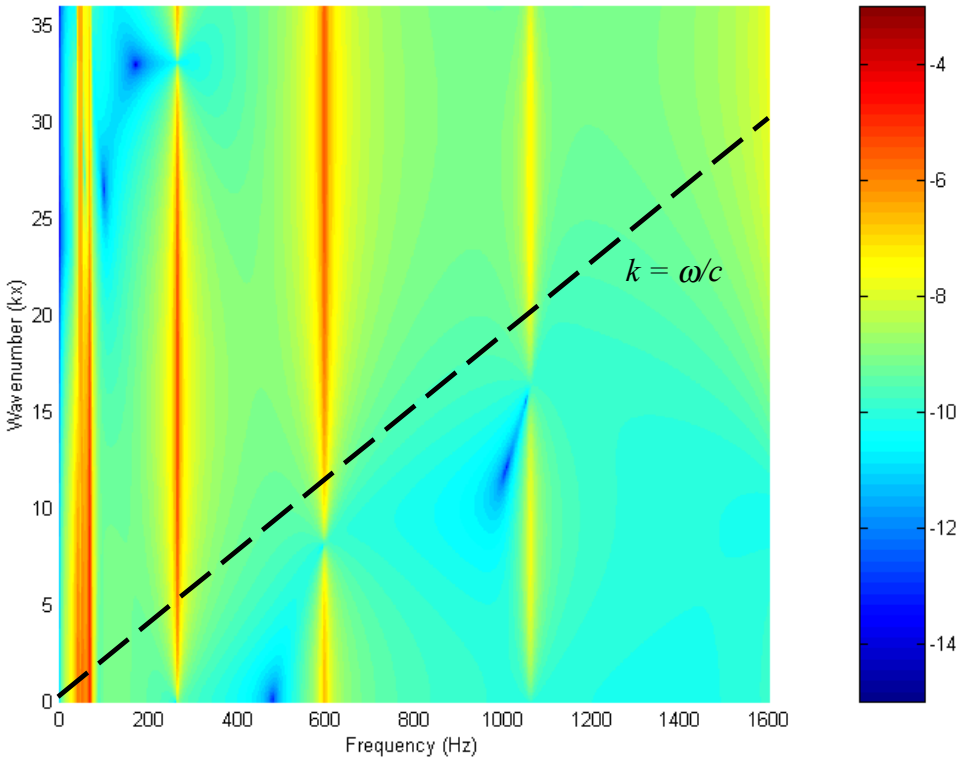

Figure 3.19: Wavenumber spectrum of treated beam for frequency band 0–1600 Hz.

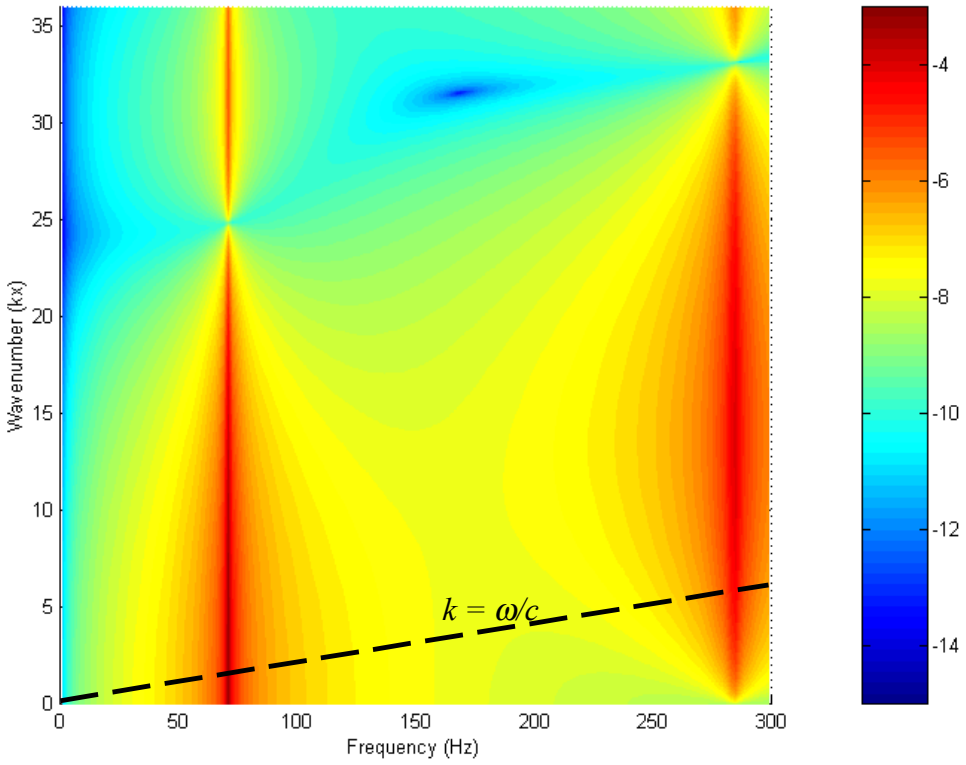

Figure 3.20: Wavenumber spectrum of untreated beam for frequency band 0–300 Hz.

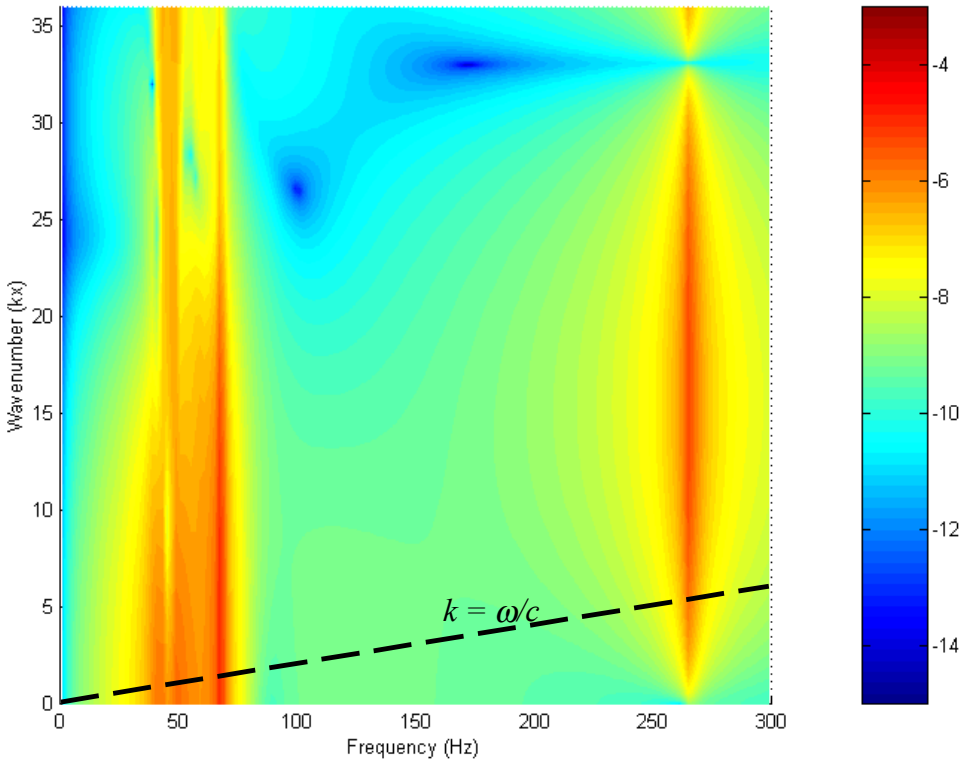

Figure 3.21: Wavenumber spectrum of treated beam for frequency band 0–300 Hz.